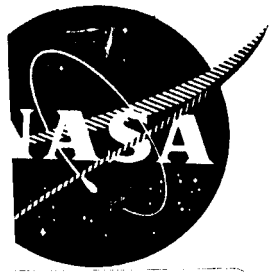

NASA CR-54740
WCAP-2923

IN-PILE MEASUREMENT OF UO_2 THERMAL CONDUCTIVITY

by

M. G. Balfour, J. A. Christensen, and H. M. Ferrari

prepared for

NATIONAL AERONAUTICS AND SPACE ADMINISTRATION

CONTRACT NAS 3-4589-PB

WESTINGHOUSE
ATOMIC POWER DIVISION

NASA-CR 54740
WCAP-2923

Final Report

IN-PILE MEASUREMENT OF UO_2 THERMAL CONDUCTIVITY

by

M. G. Balfour, J. A. Christensen, and H. M. Ferrari

prepared for

National Aeronautics and Space Administration

March 1, 1966

Contract NAS 3-4589-PB

Technical Management
NASA Lewis Research Center
Cleveland, Ohio
Technical Liason Office
Dominic C. DiIanni

Westinghouse Atomic Power Division
Pittsburgh, Pa. 15230

In-Pile Measurement of UO_2 Thermal Conductivity

by

M. G. Balfour, J. A. Christensen,* and H. M. Ferrari

Abstract

21727

In-pile effects of stoichiometry and grain growth on UO_2 thermal conductivity were studied in instrumented fuel capsules. Results show that columnar grain growth has no significant effect on heat transfer in UO_2 fuels. Migration of lenticular voids during irradiation was shown to have an important effect on fission product redistribution. Irradiation of a $UO_{1.941}$ capsule showed a mean thermal conductivity nearly 20 percent higher than in a $UO_{2.005}$ capsule under similar conditions.

Author

*Now employed at Battelle-Northwest Laboratories, Richland, Wash.

Table of Contents

List of Figures (P. 29-47)

Figure

List of Tables

I. INTRODUCTION

A. Background

Uranium dioxide thermal conductivity is a critical parameter in the design of high-performance reactor fuel elements utilizing this material in bulk form. Dimensional stability, fission gas release, and special requirements for fuel containment are highly temperature-dependent and determined principally by operating power level and fuel thermal conductivity. Due to these factors it is highly important to obtain direct, precise measurements of thermal conductivity and a thorough understanding of the basic mechanisms responsible for in-pile behavior of UO_2 fuels.

There has been an intensive investigation of UO_2 thermal conductivity in both in-pile and out-of-pile tests in recent years. However, the nature of the material has made it extremely difficult to obtain accurate and comprehensive information. UO_2 is highly refractory (melting point 2800°C) and is used as a fuel at temperatures up to or exceeding melting. The relatively low thermal conductivity results in steep thermal gradients in conventional rod-type elements. In addition, the compositional and structural changes associated with fission heating further complicate heat transfer within operating fuel elements. These changes unfortunately are not reproducible under laboratory conditions, therefore making out-of-pile experiments of limited value for design purposes.

In-pile thermocouple measurements of UO_2 thermal conductivity have generally been limited[1-9] to relatively low-temperature measurements. This reflects the inability of thermocouples to withstand the high temperature ($T>1600°C$) UO_2 environment for significant periods of

time. High-temperature thermal conductivity has had to be inferred from the examination of irradiated fuel cross-sections involving assumptions as to the temperatures required to cause microstructural changes during irradiation. A lack of precision has been the rule.

Laboratory data on the high-temperature thermal conductivity of UO_2 single crystals[10] have led to the postulate that microstructural changes occurring during irradiation grossly alter the thermal conditions existing within bulk UO_2 fuel elements.[13] Extrapolation of the single-crystal data suggests that the thermal conductivity of UO_2 single crystals above 1800°C is five to ten times greater than that of polycrystalline material. If this is so, the in-pile formation of an essentially single-crystal columnar grain structure in UO_2 fuels should result in a marked decrease in fuel temperatures. This increase in thermal conductivity in regions of grain growth was originally postulated to result from enhanced radiant heat transfer.[11] However, recent theoretical analyses[12] of heat transfer mechanisms in UO_2 refute this explanation.

The formation of long, porosity-free columnar grains in UO_2 fuel rods is believed to be caused by migration of voids toward the fuel center by a vapor-condensation mechanism.[13,14] The UO_2 vaporizes on the hot edge of such a void, diffuses through the gaseous medium within the void, and condenses on the cold side, causing a net mass movement. Although this theory has been employed to analyze the thermal behavior of fuel elements,[13] the effect of void size on migration rates is not known, nor is their genesis fully understood.

Other studies indicate that slight variations in stoichiometry may grossly affect heat transfer. Out-of-pile measurements[15,16,17] have shown that the thermal conductivity of UO_2 is enhanced or depresed by lowering or raising, respectively, the O/U ratio of the

specimen. A significant increase in thermal conductivity above 1400°C in a $UO_{1.99}$ specimen[15] was attributed to a high-temperature electronic contribution to heat transfer. By properly adjusting the initial stoichiometry in UO_2 fuel, it may be possible to significantly improve fuel element performance. Theoretically, the heat rating for center melting in hypostoichiometric fuels approaches 150% of that in conventional, stoichiometric or slightly hyperstoichiometric uranium dioxide[18].

Recent in-pile experiments[19] show an improvement in thermal conductivity for UO_{2-x} at temperatures around 1200°C. However, this probably is due to radiant transfer, since an electronic contribution to UO_2 thermal conductivity should not be significant below 1400°C.

B. Experimental Objectives

The experiment was designed to measure and analyze the temperature distributions in UO_2 fuel elements during operation. The experiment was primarily concerned with thermal effects, rather than irradiation effects. Specifically, the experimental objectives were:

1) To obtain direct measurements of UO_2 thermal conductivity in-pile to high temperatures (>2000°C).
2) To determine the effect of columnar grain growth on thermal conductivity.
3) To determine the effect of void size and distribution on the formation of columnar grains.
4) To test the hypothesis that electronic heat transfer in hypostoichiometric UO_2 can significantly improve fuel element performance.

II. Experimental Apparatus

A. General Description

Three instrumented test capsules were irradiated for one to two days in the beryllium reflector of NASA's Plum Brook Reactor (Figure 1).

Capsule I was irradiated in the RA6 test hole, and Capsule II and III in RA6 and RA3, respectively. Each capsule was of the same physical design (Figure 2) and contained seven W-5% Re/W-26% Re thermocouples uniformly distributed in the UO_2 fuel, plus three Chromel-Alumel thermocouples in the annular NaK calorimeter. Included in the test were:

1) A single capsule designed to operate at 18 kw/ft for 24 hours. The purpose was to determine the thermal conductivity of the UO_2 fuel by measuring continuously the temperature variation. The effect of columnar grain formation on thermal conductivity was to be determined. In addition, a fuel pellet was drilled with holes of various sizes and locations to investigate void migration kinetics (Figure 5A).

2) Two capsules, one fueled with $UO_{2.005}$ and the other with $UO_{1.941}$, each designed to operate at 22 kw/ft for 50 hours. This test was intended to show whether or not hypostoichiometry in uranium dioxide contributes to a substantially improved thermal conductivity, as suggested by out-of-pile experiments.

B. Experimental Assembly

The experimental assembly comprised: (1) the capsule proper consisting of an outer support or basket and an inner capsule assembly containing the thermocoupled UO_2 fuel; (2) a lead tube section extending from the capsule through a reactor instrumentation port to a location exterior to the reactor pressure vessel; (3) thermocouple terminal assembly (Figure 1) and (4) appropriate instrumentation to permit continuous recording of the fuel temperatures during irradiation.

The capsules were irradiated in the beryllium reflector. The capsule and capsule holder assembly were designed to replace the existing beryllium RA hole plug. Heat generated in the fuel pins was removed by the primary coolant water ($\sim$135°F.) flowing upward around the capsule at an estimated 27.2 gpm with a 5.0 psi pressure drop. The principal components in the inner capsule assembly included the fuel pellets, the inner and outer fuel cans, and the thermocouples.

Cold-worked (10%) type 348 stainless steel tubing was used for both the primary and secondary fuel cladding; the wall thicknesses were 0.025 inches and 0.050 inches respectively. The end plugs were machined from ASTM A276 type 304 stainless steel. The two cans were separated by a 0.060 inch annulus filled with NaK (44% Na-56% K) which served as a heat transfer media and calorimeter.

The cold fuel-to-clad diametral gap was nominally 0.025 inches. Helium at one atmosphere pressure was introduced into the inner fuel can during the final seal welding. Normal operating pressure for this gas was 1.8 atmospheres.

Six tantalum-sheathed, W-5% Re/W-26% Re thermocouples were positioned in the fuel at two radial positions on three radii spaced 120° apart, as shown in Figure 3. A similar W-26% Re-sheathed thermocouple was located at the fuel center line. The thermocouple wells were ultrasonically drilled in the fuel pellets to a diameter of 0.068 inches.

The thermocouple probe sheaths were 0.062 inches in diameter with a wall thickness of 0.012 inches. The thermocouple probe sections were insulated with vitrified BeO and had grounded hot junctions to provide rigid mechanical support for the brittle tungsten thermoelement near the weld region.

The thermocouple extension sheaths were of type 348 stainless steel and the transition from the refractory metal probe sheaths was accomplished by an interference fit and an "A" nickel braze. In addition, three 0.042 inch diameter stainless steel sheathed Chromel-Alumel thermocouples were positioned in the sodium annulus in the same relative positions as the fuel thermocouples.

All joints in this assembly were tungsten-inert-gas welded with the exception of the extension sheath to probe transition discussed above. The complete thermocouple-end plug assembly, consisting of seven refractory metal thermocouples, three Chromel-Alumel thermocouples, and inner and outer end plugs, was supplied as a fabricated assembly by the vendor. The assembly was completely unitized in construction (Figure 4).

A multichannel strip chart recorder was used to continuously monitor the output from the fuel thermocouples. This instrument functioned solely as a recorder and was not interconnected with any reactor instrumentation. A second multichannel recorder was used to monitor the three Chromel-Alumel thermocouples immersed in the NaK annulus. Additional instruments required for the experiment included a precision potentiometer for calibration checks on the thermocouple output recorder, and an ohm-meter to check thermocouple continuity after installation of the capsule in the reactor.

C. UO_2 Design Parameters

1. Physical Parameters

The fuel section in each capsule contained a column of nine UO_2 pellets, each nominally 1.250 inches in diameter and 0.5 inches long (total fuel length of 4.5 in.). Detailed dimensions are given in the Appendix. Capsule I contained 95% T. D. $UO_{2.005}$ containing 0.64 w/o U-235. Capsule II fuel was identical except for an enrichment of 0.82 w/o U-235. Capsule III contained

0.82 w/o U-235, with an o/u ratio of 1.941 in the seven center pellets, with $UO_{2.005}$ end pellets. Capsules I and II each contained one pellet (#6) in which spirally distributed artificial voids were drilled ultrasonically in the pellet face to diameters of 0.010, 0.020, and 0.040 inches, and to a depth of 0.094 inch. Figure 5A shows this pellet in Capsule I before irradiation.

2. Thermal and Irradiation Design

The design heat ratings are given in Table I, along with irradiation time and reactor cycles.

TABLE 1

IRRADIATION DESIGN PARAMETERS

	Reactor MW	Kw/ft	Irradiation Time (Hours)	Reactor Cycle
Capsule I, $UO_{2.005}$	33.3	18	24	25
Capsule II, $UO_{2.005}$	39.0	22	50	27
Capsule III, $UO_{1.941}$	39.0	22	50	27

Variable reactor power was scheduled to provide sufficient flexibility to achieve the desired UO_2 operating power and temperatures. Final reactor power levels (MW) were selected from the observed temperatures as the reactor was brought up to power in steps. In order to achieve identical heat ratings in the latter two capsules, they were irradiated simultaneously in symmetrical flux positions (RA6 and RA3).

To offset the extreme neutron gradients in this region, a boronated stainless steel liner of variable thickness, designed to flatten the flux within the capsules, was added to the flow basket which supports the experimental capsules. Boron distribution was determined from calculations and from mockup experiments.

III. EXPERIMENTAL RESULTS

A. Time - Temperature Measurements

1. Capsule I was irradiated during October, 1964, for a period of 24 hours. Time-temperature-reactor power relationships are shown in Figure 6. It was necessary to go to higher reactor and fuel power levels than intended (Table 1) to achieve the desired UO_2 operating temperatures (>2000°C). All ten thermocouples performed satisfactorily during the first seven hours of the test. During this period, the center temperature was increased to 1750°C, held constant at this temperature for 90 minutes, and then quickly increased to 2030°C. Although extensive columnar grain growth occurred, no evidence of an elevated temperature increase in thermal conductivity during irradiation was observed. Figure 6 shows a slight increase in fuel temperature with time which reflects the slight upward neutron flux drift which occurred during the test, as verified by a gradual increase in the temperature gradient between the NaK and the cooling water.

   At peak power, two of the three "inner ring" thermocouples operating at 1850°C began to drift slowly downward until they stabilized, after 6 hours, at 1600°C. This must be interpreted as failure of these thermocouples since their behavior is anomalous with respect to the other five couples in the fuel and since other laboratories have observed similar behavior of these thermocouples at 1850°C and above. Such "failures" may be related to tantalum diffusion from the sheath to the grounded hot junction with a resulting change in thermoelectric characteristics.

2. Capsules II and III were irradiated at 25 Kw/ft peak power levels for thirty hours. During this period, maximum fuel center temperatures of 2300°C were measured in both capsules (Figures 7 and 8). The capsules operated at heat ratings which differed by

less than 6% (the maximum sensitivity of the NaK calorimeters). This close flux control was achieved by using symmetrical reflector positions and by special loading of the reactor core. Some compensation for flux assymmetry could be achieved by adjusting shim rod positions; however, this additonal flexibility proved unnecessary. As with Capsule I, no apparent change in UO_2 thermal conductivity occurred during irradiation. On approach to power, the $UO_{1.941}$ (Capsule III) operated, as expected,* at slightly lower temperatures than did the $UO_{2.005}$ (Capsule II). When reactor power stablized at 53 MW, however, temperatures were nearly identical in both fuel cores. Shortly thereafter, the center thermocouple in Capsule III failed. This contrasts with the performance of the W-26% Re-sheathed center couples in Capsules I and II which gave reliable outputs for 24 and 26 hours, respectively.

B. Post-irradiation Examination

After irradiation each capsule was inspected, measured, and sectioned for burnup analysis and metallography.

1. Dimensional Measurements

The length and diameter of the inner capsules were measured and are included in Table A-1 (Appendix), along with pre-irradiation measurements. No significant changes were observed.

2. Burnup Analysis

Cesium-137 analysis for the three capsules (pellets #2,8) are listed:

---

*Cf. part IV. D-2

TABLE 2

UO_2 BURNUP ANALYSIS:

Capsule	Cs^{137} (dpm/gU)	Average Burnup: fissions/cc	Mwd MTU
I	5.94×10^7 6.85×10^7	2.18×10^{17}	7.93
II	1.24×10^8 1.14×10^8	4.08×10^{17}	14.84
III	1.15×10^8 1.41×10^8	4.39×10^{17}	15.96

The calculations were based upon fission yields given by Katcoff.[21]

3. Metallography

Metallographic samples were taken at the thermocouple hot junctions of capsules I, II, and III as shown in Figures 9, 10, and 11, respectively. As Figure 9 shows, the inner ring thermocouples are situated at the outer terminus of the columnar grain region in Capsule I.

Other cross sections show a slight increase in the diameter of the columnar grain region toward the bottom of Capsule I. Apparently the tapered, boronated sheath used to suppress the anticipated axial flux gradient was not completely effective. At a position 1/2 inch above the bottom of the fuel stack, columnar grains as long as 1/4 inch occupy 65% of the fuel diameter (Figure 12). An autoradiograph from this section is shown in Figure 13. The columnar grains in Capsule I are not quite symmetrical geometrically, indicating that a slight skew in the neutron flux existed. The extent of grain growth in Capsules II and III is essentially identical and somewhat exceeds that demonstrated by Capsule I.

IV. RESULTS AND DISCUSSION

A. Heat Transfer in Columnar Grains

The time-temperature plot from Capsule I (Figure 6) shows that the UO_2 was slowly brought to a center temperature of 1750°C, the approximate threshold for columnar grain formation. Reactor power was then rapidly increased until the coolest inner ring thermocouple reached 1720°C and the corresponding center temperature was 2030°C. These conditions were maintained for 18 hours while all thermocouples were monitored with recording instruments. During this period, an increase of approximately 100°C occurred in all fuel temperatures. This increase was probably due to irradiation effects on conductivity in the relatively cool outer regions of the fuel in addition to the observed upward trend in the reactor flux level. Two of the inner ring thermocouples failed about one hour after power stabilization, possibly due to tantalum contamination of the grounded hot junction. However, the center thermocouple, sheathed in W-26% Re, and the coolest inner ring thermocouple performed perfectly throughout as did the NaK thermocouples.

Post-irradiation metallography (Figure 9) showed that one inner ring thermocouple was situated exactly at the outer edge of the columnar grains. This proved to be the only such thermocouple which did not fail, and thus a continuous measurement of the temperature increment ΔT across this region was obtained. The change in ΔT can be precisely correlated with change in thermal conductivity if the measurements are normalized to the ΔT existing at the onset of columnar grain growth. This has been done in Table A-2, in which the initial mean thermal conductivity across the columnar grain region, Δr, is $\bar{K}_o \sim \frac{(kw/ft)_o}{(\Delta T)_o} \Delta r$. Ratioing this with mean conductivity at a later time, t, gives the relative change: $\bar{K}_t / \bar{K}_o = \frac{(KW/ft/\Delta T)_t}{(KW/ft/\Delta T)_o}$ as a function of time. The data have been plotted in Figure 14, along with maximum error limits, and show that the change in thermal conductivity due to columnar grain growth is only a ($4 \pm 2\text{-}1/2\%$)

increase. This is very small compared with the increase postulated (10, 13) for radiant transmission through columnar grains, and probably reflects a combination of fuel densification and the positive temperature coefficient for UO_2 conductivity above approximately 1400°C. The results of this test thus show that columnar grain growth has essentially no effect on heat transfer in UO_2 fuels.

This experiment has also provided the first direct measurements of the temperature threshold for in-pile columnar grain formation. Nine different radial thermal gradient measurements yielded columnar grain growth temperatures between 1700° and 1900°C, with a mean of 1760°C.

B. Effect of Artificial Voids

The effects of irradiation on void size and distribution are illustrated in Figure 5B for Capsule I. Voids within the columnar grain region tended to elongate along the fuel radius. Voids near the cooler edge of the recrystallized region migrated toward the fuel center, while those initially near the center appear relatively immobile. This agrees with analytical predictions of void migration rates, approaching zero as the thermal gradient goes to zero.[13] No effect of void size on migration rate was observed. Some of the artificial voids in the columnar grain region were partially intact even though they were surrounded by well developed columnar grains. This suggests that mechanisms other than void migration are important in forming columnar grains. Voids outside the columnar grain region were unchanged in size and position, as expected.

The most significant feature in Figure 5B is the degeneration of some of the artificial voids initially located near the fuel center into aggregates of smaller, lenticular voids. These voids subsequently migrated toward the center carrying fission fragments with them as evidenced by the activity depletion in the fuel regions

through which the voids have passed (Figure 5C). This observation is important because it establishes the feasibility of spawning mobile voids from relatively large internal cavities. Thermally-induced cracks should make the most important contributions to this mechanism; in fact, the circumferential cracks frequently observed in irradiated UO_2 fuel cores may be the principal source of migrating voids. This premise would explain why columnar grains are often widest at their point of origin rather than tapered at both ends as they should be if their formation required coalescence of fine porosity into relatively large lenticular voids. This mechanism also qualifies migrating voids as vehicles for fission fragment redistribution since each thermal cycle of the fuel creates thermal cracks which can propagate new generations of migrating voids in fuel cores having significant prior burnup.

The autoradiograph of the spirally drilled pellet, shown in Figure 5C, shows depletion of fission fragments in the recrystallized portion of the fuel. This region is bounded by a band of high activity approximately 0.1 cm. wide. The cooler fuel regions have an intermediate, uniform activity.

Figure 12 illustrates the maximum fuel grain growth which occurred in Capsule I. The corresponding autoradiograph (Figure 13) shows several clearly defined radial variations in fission fragment concentration. Particularly interesting is the annular activity-depleted region immediately adjacent to the fuel center. The occurrence of this region tends to confirm theoretical predictions that void migration rates are a maximum at some finite radius and not at the fuel center[13]. The region of maximum void velocity should thus contain relatively few of those fission fragments which are carried along by the moving voids. The center of the rod shows

an aggregation of lenticular voids, which supports the theoretical predictions that void migration velocity reaches zero at the thermal center. The role of these voids in carrying fission fragments is borne out by the fact that they can be seen distinctly in this autoradiograph.

C. Integrated Thermal Conductivity

Figures 15 and 16 show $\int_{600}^{Tc} K_{2.005}\, dT$ for Capsules I and II, respectively. The out-of-pile data of Godfrey and McElroy[19] are used for low temperatures ($T < 1100^{\circ}C$). The values of the integral as a function of temperature were computed from the well-known relationship[22]:

$$\int_{T_s}^{T_r} K dT = \frac{q}{4\pi} \left\{ \frac{I_o(\kappa a) - I_o(\kappa r)}{(1/2)\kappa a \quad I_1(\kappa a)} \right\}$$

where T_r = UO_2 temperature at a radius r from the center, $^{\circ}C$

T_s = UO_2 surface temperature, $^{\circ}C$

a = Fuel radius, cm

K = Thermal conductivity of UO_2, w/cm $^{\circ}C$

q = Linear power rating, w/cm

κ = Inverse diffusion length, cm^{-1}

I_o, I_1 = Modified Bessel functions (1st kind) of zero and first order, respectively

Values of the dimensionless quantity (κa) used for Capsule I (0.64 w/o U-235) and Capsule II (0.82 w/o U-235) were κa = 1.90 and 2.05, respectively. "Selni" cross-sections and the Wigner "rational approximation" were used to derive the values of κ employed in these calculations[26].

Power levels were computed from Cs-137 burnup data and gamma heating estimated from critical experiments in the Mockup Reactor (MUR). Time-average peak power levels were:

Capsule I	22.0 ± 1.1 kw/ft
Capsule II	23.6 ± 1.6 kw/ft
Capsule III	25.1 ± 1.7 kw/ft

Variation of power as a function of time was determined from the changes in coolant and NaK calorimeter temperatures, the difference of which is proportional to power level, ie, $q \sim (\Delta T)_{NaK-H_2O}$. Values of ΔT vs time are shown in the time-temperature plots, Figures 6, 7, 8. Although the Cs-137 analysis in Capsule II showed a lower power rating, this is believed to be in error because of center melting* and subsequent axial fission product redistribution. Within the limits of calorimetry (~6%) the power level was the same in Capsules II and III, and for purposes of comparing the two a common value of 25.1 kw/ft was assumed.

Tables of $\int k dT$ values for all three capsules are included in the appendix for temperatures measured at the seven thermocouple positions within the fuel. Variations within each of the clusters of three thermocouples at the half-radius and edge of the fuel, respectively, are due to corrections for a slight flux assymmetry, as revealed by post-irradiation metallography (Figures 9, 10, 11).

The error band for Capsule I (Figure 15) includes the maximum error due to the following factors:

1) Uncertainty in radial thermocouple locations. Since the thermocouples had grounded hot junctions, this error is assumed to be equal in magnitude to the entire width of the thermocouple wells, 0.068 in.

*Discussed in Section D-1.

2) Uncertainty in thermocouple calibration, ± 1%

3) Strip chart data uncertainty: ± 0.05 mv

Because of the large error inherent in absolute measurement of $\int KdT$ (~25%), no attempt was made to derive a thermal conductivity curve, K(T) vs T, from Figures 14 or 15. The error bands for Capsules II and III do not include uncertainty in power level, which is assumed to be the same for both capsules.

Figure 16 gives $\int K_{1.94} dT$ vs T for Capsule III. The curve was derived by calculating fuel surface temperatures using gap conductances deduced from the Capsule II data. Since the diameter of the $UO_{1.941}$ pellet at the thermocouple hot junctions shrank to 1.2477 in. during the reduction annealing process, surface temperatures were over 100°C higher at full power than in Capsule II.

D. Effects of Stoichiometry on Fuel Performance

1. Morphological Effects

The extent of grain growth in Capsules II and III is essentially the same (Figures 10 and 11). One difference in grain morphology was observed in comparing the UO_2 with the UO_{2-x} fuel. Columnar grains in the UO_{2-x} are relatively very narrow, much like those observed in high burnup fuels. This may be associated with the high concentration of uranium metal precipitates present in the UO_{2-x} in Capsule III and generally found in high burnup UO_2.

Examination of the cross-section of Capsule II (Figure 10) reveals a second-phase region about the center of the pin. This is probably due to impurities which recrystallized from a low-temperature melting zone formed when the inner four thermocouples reacted with the UO_2 fuel. These thermocouples were completely dissolved, as no trace could be found of them in

this metallographic specimen. Apparently UO_2 stoichiometry influences compatibility with the refractory metal thermocouple components. This is substantiated by the observation of apparently satisfactory performance of tantalum sheathed thermocouples at temperatures to 2100°C in UO_{2-x}. These thermocouples invariably failed above 1900°C when used in contact with stoichiometric UO_2.

2. Heat Transfer

The increased thermal conductivity of UO_{2-x} observed at high temperatures in out-of-pile experiments (15, 16) is thought to reflect an electronic contribution to heat transfer. The theoretical expression for this component is:

$$K_e = 2\left(\frac{K}{e}\right)^2 T\left[\sigma + \frac{2\sigma_n\sigma_p}{\sigma}\ (Eg/2kT + 2)^2\right]$$

where: K_e = electronic thermal conductivity component
k = Boltzmann constant
e = Charge on a charge carrier
T = Temperature (°K)
σ_p = electrical conductivity due to holes
σ_n = electrical conductivity due to electrons
$\sigma = \sigma_n + \sigma_p$, total electrical conductivity
Eg = Activation energy for exciting an electron into the conduction band.

The total thermal conductivity for UO_{2-x} excluding radiant effects is the above expression plus the conductivity due to phonon transfer,

$$\text{i.e. } K \text{ total} = K_{ph} + K_e.$$

Christensen[12] has calculated the maximum electronic contribution to thermal conductivity (assuming $\sigma_p = \sigma_n$), taking values of Eg/2 = 0.95 ev and electrical conductivity data from Wolfe[23]. The electronic component is not significant below ~1400°C but might be very substantial in highly rated fuel elements. It has been estimated[18] that the heat rating necessary to cause center melting in a fuel core could be increased up to 50% if the maximum electronic contribution were realized.

Conventional stoichiometric or slightly hyperstoichiometric UO_2 fuels do not demonstrate this increased conductivity, however, despite evidence that uranium dioxide becomes substoichiometric in those regions exceeding ~1500°C during irradiation[24]. One possible explanation for this is that oxygen evolved by thermal reduction in the hot, central regions of a fuel pin is gettered in the cooler surrounding regions (below 1500°C). Thus a compositional gradient would exist radially across the fuel, from UO_{2-x} near the center to UO_{2+x} at the edge. Since excess oxygen reduces thermal conductivity[17], the electronic contribution at high temperatures might be masked by less efficient heat transfer in the hyperstoichiometric region. It has been postulated[18] that this situation could be obviated by using sufficiently hypostoichiometric fuel to prevent the O-U ratio from exceeding 2.00 in the low-temperature regions during irradiation. The fuel in Capsule III was chosen as $UO_{1.941}$, which by the temperature-oxygen pressure-composition phase diagram[25] should satisfy this condition.

Comparison of the nominal $\int KdT$ curves in Figures 15 and 16 gives

$$\int_{600}^{2250} K_{2.005}\, dT = 41.4 \text{ w/cm and } \int_{600}^{2250} K_{1.941}\, dT = 49.0 \text{ w/cm.}$$

Thus, if one ratios the average thermal conductivities between 600 and 2250°C, one obtains a nearly 20% higher thermal conductivity for the hypostoichiometric fuel, viz. $\overline{K}_{1.941}/\overline{K}_{2.005} = 1.184$.

From calculations of the maximum electronic contribution to thermal conductivity[12], $\int_{600}^{2250} K_{el}\, dT \simeq 7$ w/cm. Comparison of the nominal curves in Figures 14 and 15 gives a difference in integrated conductivity of ∿7.6 w/cm at 2250°C. This is approximately the same as one calculates for the postulated high-temperature electronic contribution. Thus, the experimental results are consistent with the hypothesis that use of hypostoichiometric fuel enables a high-temperature enhancement of thermal conductivity to be exploited in-pile.

V. SUMMARY OF RESULTS

A. Columnar Grain Effects

The effect of in-pile columnar grain growth on UO_2 thermal conductivity was a $(4 \pm 2.5)\%$ increase. This is very small when compared to the increases from radiant transmission through columnar grains postulated by previous investigators. The small increase observed can be explained by fuel densification and a positive temperature coefficient for UO_2 thermal conductivity above 1400°C. The results of this test show that columnar grain growth has essentially no effect on heat transfer in UO_2 fuels.

B. Void Migration Effects

The effect of irradiation upon voids artificially drilled into the face of a fuel pellet prior to irradiation was studied. Voids located outside the columnar grain region were unchanged in size and position whereas voids within the columnar grains tended to migrate toward the center and change their shape. Autoradiographs indicate that artificial voids near the center engendered small lenticular pores which carried away fission products, leaving behind depleted regions. The pattern of fission product redistribution by lenticular pores seems to confirm the theoretical mechanism of UO_2 vaporization-condensation within the pores.

C. Integrated Thermal Conductivity

Integrated conductivity curves were drawn from temperature and power measurements for Capsules I and II, containing $UO_{2.005}$. Because of low precision associated with these measurements, no attempt was made to obtain a thermal conductivity curve by differentiation.

D. Effects of Stoichiometry

The mean thermal conductivity of $UO_{1.941}$ between 600 and 2250°C was nearly 20% higher than in $UO_{2.005}$ irradiated under the same power conditions. The results are consistent with a theoretical ambipolar electronic contribution to thermal conductivity at high temperatures.

VI. ACKNOWLEDGEMENTS

The authors are indebted to Mr. P. M. Maxin, who tabulated the experimental data and helped prepare this report.

VII. REFERENCES

1. Cohen, I., Lustman, B., Eichenberg, J. D., "Measurement of the Thermal Conductivity of Metal-Clad UO_2 Rods During Irradiation", WAPD-228 (1960)

2. Daniel, R. C., Cohen, I., "In-Pile Thermal Conductivity of Oxide Fuel Elements to High Fission Depletions", WAPD 246-(1964)

3. Robertson, J. A. L. and Hawkings, R., "Thermal Conductivity of UO_2 Under Irradiation: Some Early Results", AECL-1733 (1963)

4. Robertson, J. A. L., Ross, A. M., Notley, M. J. F., MacEwan, J. R., "Temperature Distribution in UO_2 Fuel Elements", J. Nucl. Mat., Vol. 7 No. 3 (1962) p. 225-262

5. Robertson, J. A. L., "High Temperature Properties of Ceramic Fuels: Their Significance and Measurement", AECL-1529 (1962)

6. Clough, D. J., "Effect of Burnup on the Thermal Conductivity of Stoichiometric Sintered UO_2", AERE-R-4146 (1962)

7. Clough, D. J., Sayers, J. B., "The Measurement of the Thermal Conductivity of UO_2 Under Irradiation in the Temperature Range 150°C - 1600°C", AERE-R-4690 (December 1964)

8. Coplin, D. H., Hausner, H., Lyons, M. F., Weidenbaum, B., "In-Pile Direct Measurement of UO_2 Thermal Conductivity", Trans. ANS, Vol 8, No. 1, p. 35, (1965)

9. Bogaievski, M., et al, "Direct Measurement of the Thermal Conductivity of UO_2 In-Pile to 1200°C", Paper CN-16/10, Prague (1963)

10. Daniel, J. L., Matolich, J.,Jr., and Deem, H. W., "Thermal Conductivity of UO_2", HW-69945, Sept. 1962

11. Bates, J. L., "Thermal Conductivity of UO_2 Improves at High Temperatures", Nucleonics, 19 (6) p. 83-87 (June 1961)

12. Christensen, J. A., "Thermal Conductivity of Nearly Stoichiometric UO_2- Temperature and Compositional Effects", WCAP-2531 (Nov. 1963); also Trans. ANS. 7, No. 1, p. 128 (June 1964)

13. DeHalas, R., and Horn, G. R., "Evolution of Uranium Dioxide Structure During Irradiation of Fuel Rods", J. Nucl. Mat., 8, No. 2, (1963), p. 207-220

14. MacEwan, J. R., and Lawson, V. B., "Grain Growth in Sintered Uranium Dioxide: II, Columnar Grain Growth", J. Amer. Cer. Soc, 45 (1962) p. 42

15. Christensen, J. A., Bush, A. J., Ferrari, H. M., and Allio, R. J., "Uranium Dioxide Thermal Conductivity", Trans. ANS, Vol 7, No. 2, p. 391-92 (Nov. 1964)

16. May, J. F., Notley, M. J. F., Stoute, R. L., and Robertson, J. A. L., "Observations on the Thermal Conductivity of Uranium Dioxide", AECL-1641, November 1962

17. Ross, A. M., "The Dependence of the Thermal Conductivity of Uranium Dioxide on Density, Microstructure, Stoichiometry and Thermal-Neutron Irradiation", AECL-1096 (Sept. 1960)

18. Christensen, J. A., "Temperature and Stoichiometry Effects on UO_2 Heat Rating", Trans. ANS, Vol. 7, No. 2 (Nov. 1964) p. 392-3

19. Robertson, J. A. L., Bain, A. S., MacEwan, J. R., and Notley, M. J. F., "UO_2 Performance - The Importance of Temperature Distribution", A/Conf. $28/^2p/17$ (1964)

20. T. G. Godfrey, and D. L. McElroy, "Thermal Conductivity of UO_2", ORNL-3372, p. 295, September 1962.

21. Katcoff, S., "Fission-Product Yields from Neutron-Induced Fission", Nucleonics, 18, No. 11 (November 1960)

22. Robertson, J. A. L., "$\int K d\theta$ in Fuel Irradiations", CRFD-835, Chalk River Ont., (1959)

23. Wolfe, R. A., "The Electrical Conductivity and Thermoelectric Power of Uranium Dioxide", WAPD-270, April 1963

24. Bates, J. L., "Metallic Uranium in Irradiated UO_2", HW-SA-3288, April 1964.

25. Alexander, C. A., and Shevlin, T. S., "Uranium Oxide Pressure-Temperature-Composition Relationships from 1000 to 2000°K", (April 1962)

26. Rose, R. G., personal communication.

APPENDIX

Tabulated Data for Capsules I, II, III

Nomenclature:

$\int KdT$ = integrated thermal conductivity, w/cm

q = linear power rating, w/cm

T_c = center temperature, °C

ΔT = temperature drop across columnar grains

T_s = fuel surface temp., °C

T_r = temperature at a radius r within fuel

r_i = inner ring thermocouple position within fuel

r_o = outer ring thermocouple position within fuel

r_1, r_2, r_3 = specific thermocouples within inner or outer rings

Thus r_{2i} refers to thermocouple #2 in the inner ring of thermocouples (see Figure 3).

Table A-1: CAPSULE DIMENSIONAL DATA

Capsule No.	Pellet Dia.	Pellet Thick.	Fuel/Clad Diam. Gap	Fuel Col. Length
I	1.250	0.460-0.510	0.0245	4.413
II	1.250	0.495-0.496	0.0245	4.459
III	1.245 - 1.250	0.483-0.495	0.0245-0.0297	4.4395

	Pre-Irrad. Clad I.D.	Pre-Irrad. Clad O.D.	Post-Irrad. Clad O.D.*	Pre-Irrad. Can I.D.	Pre-Irrad. Can O.D.
I	1.2745	1.3245	1.327-1.328	1.4459	1.544
II	1.2745	1.3244	1.326-1.329	1.4458	1.544
III	1.2745	1.3244	1.318-1.332	1.4458	1.544

*Readings taken at 0°, 90°, on four axial positions; numbers given represent the range of values observed.

Table A-2

RELATIVE CHANGE OF MEAN THERMAL CONDUCTIVITY ACROSS COLUMNAR GRAINS (CAPSULE I)

kw/ft	ΔT	$\frac{kw/ft}{\Delta T}$	$\frac{(kw/ft/\Delta T)_t}{(kw/ft/\Delta T)_o}$	Time Elapsed (Hrs) *
21.5	305	0.0705	1.000	0
21.1	294	0.0714	1.013	1/2
20.9	291	0.0719	1.020	1
20.9	290	0.0721	1.022	1-1/2
20.9	289	0.0724	1.026	2
20.9	289	0.0724	1.026	2-1/2
21.1	290	0.0726	1.030	3-1/2
21.2	292	0.0726	1.030	4-1/2
21.4	293	0.0728	1.032	5-1/2
21.5	295	0.0729	1.034	6-1/2
21.7	297	0.0731	1.038	7-1/2
21.8	299	0.0731	1.038	8-1/2
22.0	301	0.0730	1.036	9-1/2
22.1	303	0.0729	1.034	10-1/2
22.3	304	0.0734	1.042	11-1/2
22.4	306	0.0731	1.038	12-1/2
22.5	308	0.0730	1.036	13-1/2
22.7	310	0.0732	1.040	14-1/2
22.8	312	0.0731	1.038	15-1/2
23.0	314	0.0733	1.041	16-1/2

*The time is measured from the start of columnar grain formation.

Table A-3

TABULATED DATA: CAPSULE

Hours Irradiation After Startup	q w/cm	Tc, °C.	$\int_{Ts}^{Tc} KdT$ .0653 q	$\int_{Ts}^{Tr} KdT$					
				r_{1i} .0583 q	r_{2i} .0571 q	r_{3i} .0561 q	r_{1o} .0349 q	r_{2o} .0319 q	r_{3o} .0288 q
6.5	532	1750	34.74	31.02	30.38	29.85	18.57	16.97	15.32
8.0	696	2030	45.45	40.58	39.74	39.05	24.29	22.20	20.04
9.5	683	2050	44.60	39.82	39.00	38.32	23.84	21.79	19.67
12.5	695	2070	45.38	40.52	39.68	38.99	24.26	22.17	20.01
16.5	713	2089	46.56	41.57	40.71	40.00	24.88	22.74	20.53
18.0	720	2095	47.02	41.98	41.11	40.39	25.13	22.97	20.74
20.5	733	2113	47.86	42.73	41.85	41.12	25.58	23.38	21.11
24.5	752	2131	49.11	43.84	42.94	42.19	26.24	23.99	21.66

I ($UO_{2.005}$)

Tr, °C.						$\int_{Tr_o}^{Tr_i} KdT$			$\int_{Tr_o}^{Tc} KdT$		
r_{11}	r_{21}	r_{31}	r_{10}	r_{20}	r_{30}	r_1	r_2	r_3	r_{10}	r_{20}	r_{30}
600	-	1500	1122	1093	1006	12.45	-	14.53	16.17	17.77	19.45
880	1850	1720	1230	1190	1070	16.29	17.54	19.01	21.16	23.25	25.41
-	-	1750	1240	1202	1078	-	-	18.65	20.76	22.81	24.93
-	-	1770	1248	1220	1090	-	-	18.98	21.12	23.21	25.37
-	-	1788	1262	1233	1100	-	-	19.47	21.68	23.82	26.03
-	-	1793	1271	1232	1103	-	-	19.65	21.89	24.05	26.28
-	-	1810	1287	1240	1106	-	-	20.01	22.28	24.48	26.75
-	-	1818	1302	1242	1110	-	-	20.53	22.87	25.12	27.45

Table A-1

TABULATED DATA: CAP

Hours After Startup	q w/cm	Tc, °C	$\int_{Ts}^{Tc} KdT$ .0634 q	$\int_{Ts}^{Tr} KdT$							
				r_{11} .0572 q	r_{21} .0564 q	r_{31} .0548 q	r_{10} .0344 q	r_{20} .0335 q	r_{30} .0325 q	r_{11}	r_{21}
1.5	71	894	4.50	4.06	4.00	3.89	2.44	2.38	2.31	898	7
2.5	270	1399	17.12	15.44	15.23	14.80	9.29	9.05	8.78	1332	12
3.5	438	1720	27.77	25.05	24.70	24.00	15.07	14.67	14.24	1590	15
5.0	545	1904	34.55	31.17	30.74	29.87	18.75	18.26	17.71	1741	17
6.0	622	2073	39.43	35.57	35.08	34.09	21.40	20.84	20.22	1868	18
7.0	630	2089	39.94	36.04	35.53	34.52	21.67	21.11	20.48	1873	18
8.5	715	2209	45.33	-	40.33	39.18	24.60	23.95	23.24	-	18
9.5	720	2215	45.65	-	40.61	39.46	24.77	24.12	23.40	-	19
10.5	775	2239	49.14	-	-	-	26.66	25.96	25.19	-	-
11.5	778	2245	49.33	-	-	-	26.76	26.06	25.29	-	-
13.5	787	2250	49.90	-	-	-	27.07	26.36	25.58	-	-
15.5	795	2260	50.40	-	-	-	27.35	26.63	25.84	-	-
19.5	810	-	51.35	-	-	-	27.86	27.14	26.33	-	-
23.5	827	-	52.43	-	-	-	28.45	27.70	26.88	-	-
27.5	844	-	53.51	-	-	-	29.03	28.27	27.43	-	-
29.5	852	-	54.02	-	-	-	29.31	28.54	27.69	-	-

ULE II ($UO_{2.005}$)

Tr, °C				$\int_{Tr_o}^{Tr_i} KdT$			$\int_{Tr_o}^{Tc} KdT$			Ts, °C
r_{31}	r_{10}	r_{20}	r_{30}	r_1	r_2	r_3	r_{10}	r_{20}	r_{30}	
833	786	600	676	1.62	1.62	1.58	2.06	2.12	2.19	-
1256	1024	841	927	6.15	6.18	6.02	7.83	8.07	8.34	-
1505	1093	986	1035	9.98	10.03	9.76	12.70	13.10	13.53	565
1611	1123	1087	1066	12.42	12.48	12.16	15.80	16.29	16.84	526
1793	1182	1164	1123	14.17	14.24	13.87	18.03	18.59	19.21	513
1809	1191	1180	1127	14.37	14.42	14.04	18.27	18.83	19.46	513
1931	1271	1260	1194	-	16.38	15.94	20.73	21.38	22.09	480
1865	1280	1265	1190	-	16.49	16.06	20.88	21.53	22.25	480
-	1359	1322	1263	-	-	-	22.48	23.18	23.95	478
-	1382	1338	1273	-	-	-	22.57	23.27	24.05	-
-	1390	1350	1290	-	-	-	22.83	23.54	24.32	480
-	1410	1360	1300	-	-	-	23.05	23.77	24.56	-
-	1460	1390	1330	-	-	-	23.49	24.21	25.02	-
-	1490	1410	1340	-	-	-	23.98	24.73	25.55	-
-	1505	1430	1360	-	-	-	24.48	25.24	26.08	-
-	1519	1440	1371	-	-	-	24.71	25.48	26.33	-

Ta

TABULATED DA

Hours After Startup	q w/cm	Tc, °C	$\int_{Ts}^{Tc} KdT$ .0634 q	$\int_{Ts}^{Tr} KdT$						
				r_{11} .0572 q	r_{21} .0564 q	r_{31} .0548 q	r_{10} .0344 q	r_{20} .0325 q	r_{30} .0325 q	$r_{\ldots}$
1.5	71	894	4.50	4.06	4.00	3.89	2.44	2.31	2.31	
2.5	270	1348	17.12	15.44	15.23	14.80	9.29	8.78	8.78	1
3.5	438	1674	27.77	25.05	24.70	24.00	15.07	14.24	14.24	1
5.0	545	1878	34.55	31.17	30.74	29.87	18.75	17.71	17.71	1
6.0	622	2004	39.43	35.57	35.08	34.09	21.40	20.22	20.22	1
7.0	630	2023	39.94	36.04	35.53	34.52	21.67	20.48	20.48	1
8.5	715	2168	45.33	40.90	40.33	39.18	24.60	23.24	23.24	≥1
9.5	720	2168	45.65	41.18	40.61	39.46	24.77	23.40	23.40	
10.5	775	2251	49.14	44.33	43.71	42.47	26.66	25.19	25.19	2
11.5	778	-	49.33	44.50	43.88	42.63	26.76	25.29	25.29	2
13.5	787	-	49.90	45.02	44.39	43.13	27.07	25.58	25.58	2
15.5	797	-	50.40	-	44.84	-	27.35	25.84	25.84	
19.5	810	-	51.35	-	45.68	-	27.86	26.33	26.33	
23.5	827	-	52.43	-	-	-	28.45	26.88	26.88	
27.5	844	-	53.51	-	-	-	29.03	27.43	27.43	
29.5	852	-	54.02	-	-	-	29.31	27.69	27.69	

le A-5

: CAPSULE III ($UO_{1.941}$)

Tr, °C					$\int_{Tr_o}^{Tr_f} K dT$			$\int_{Tr_o}^{Tc} K dT$			Ts, °C
r_{21}	r_{31}	r_{10}	r_{20}	r_{30}	r_i	r_2	r_3	r_{10}	r_{20}	r_{30}	
806	856	643	610	740	1.62	1.69	1.58	2.06	2.19	2.19	-
1212	1202	886	881	912	6.15	6.45	6.02	7.83	8.34	8.34	-
1510	1443	1032	1040	1007	9.98	10.46	9.76	12.70	13.53	13.53	706
1713	1628	1127	1125	1074	12.42	13.03	12.16	15.80	16.84	16.84	678
1838	1757	1194	1180	1137	14.17	14.86	13.87	18.03	19.21	19.21	660
1858	1771	1204	1185	1146	14.37	15.05	14.04	18.27	19.46	19.46	660
1991	1916	1284	1248	1209	16.30	17.09	15.94	20.73	22.09	22.09	619
1991	1921	1295	1252	1209	16.41	17.21	16.06	20.88	22.25	22.25	619
2081	2010	1344	1293	1280	17.67	18.52	17.28	22.48	23.95	23.95	594
2088	2030	1367	1304	1293	17.74	18.59	17.34	22.57	24.05	24.05	-
2123	2049	1382	1313	1304	27.94	18.81	17.53	22.83	24.32	24.32	-
2145	-	1395	1335	1325	-	19.00	-	23.05	24.56	24.56	-
2240	-	1430	1350	1340	-	19.35	-	23.49	25.02	25.02	-
-	-	1445	1360	1350	-	-	-	23.98	25.55	25.55	-
-	-	1465	1375	1365	-	-	-	24.48	26.08	26.08	-
-	-	1481	1396	1382	-	-	-	24.71	26.33	26.33	-

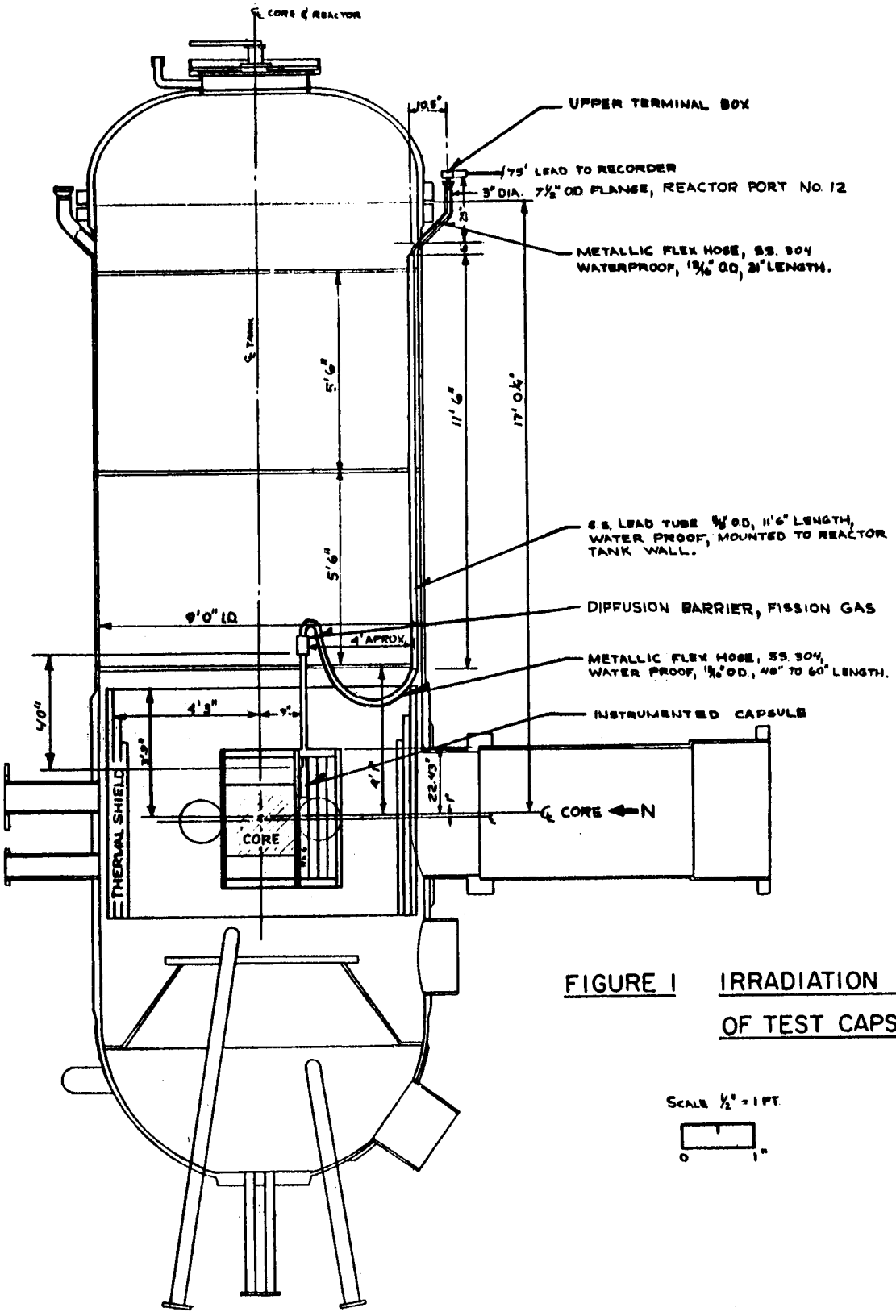

FIGURE 1 IRRADIATION POSITION OF TEST CAPSULES.

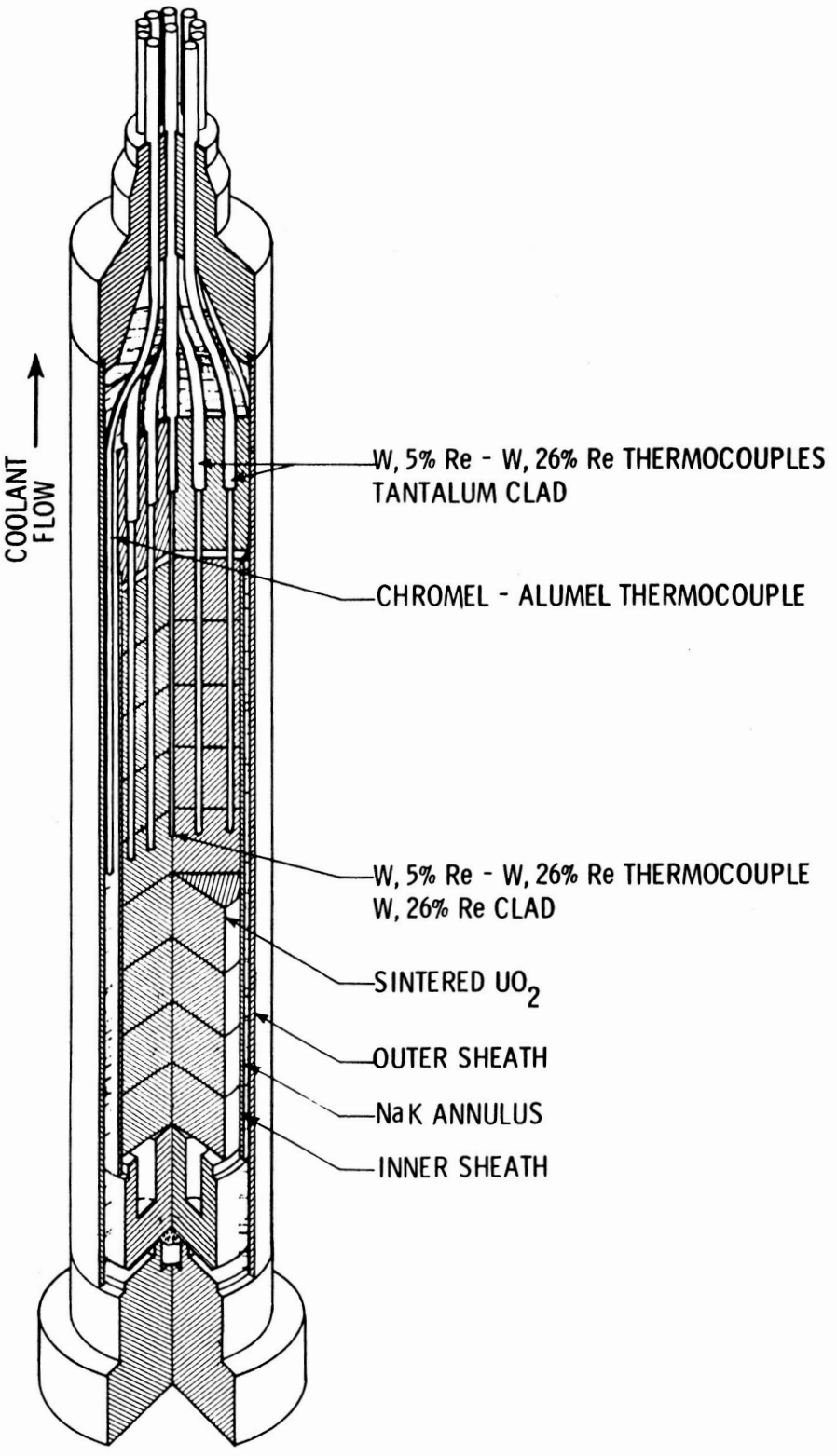

FIGURE 2

IN-PILE THERMAL CONDUCTIVITY APPARATUS.

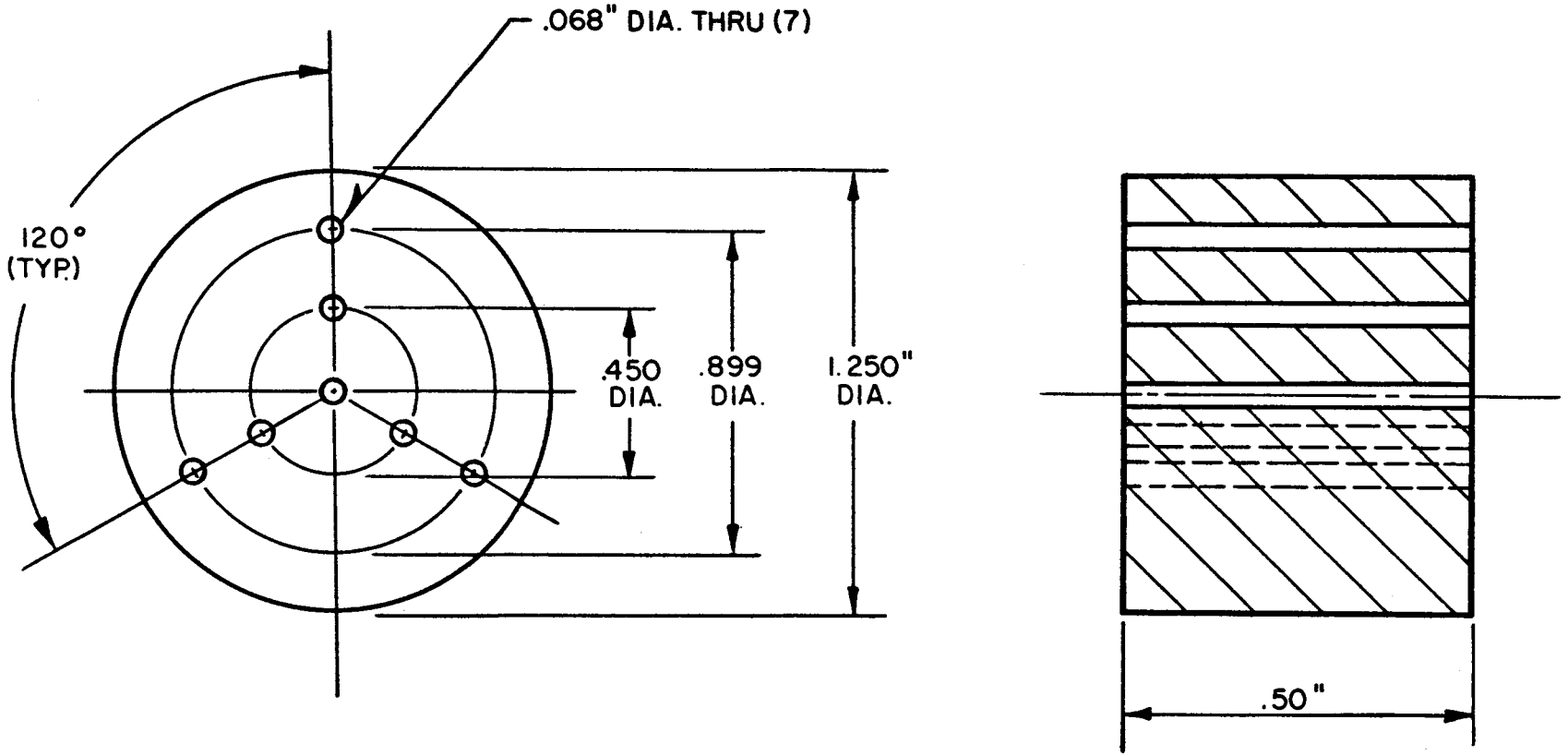

FIGURE 3 PELLET AND THERMOCOUPLE DIMENSIONS.

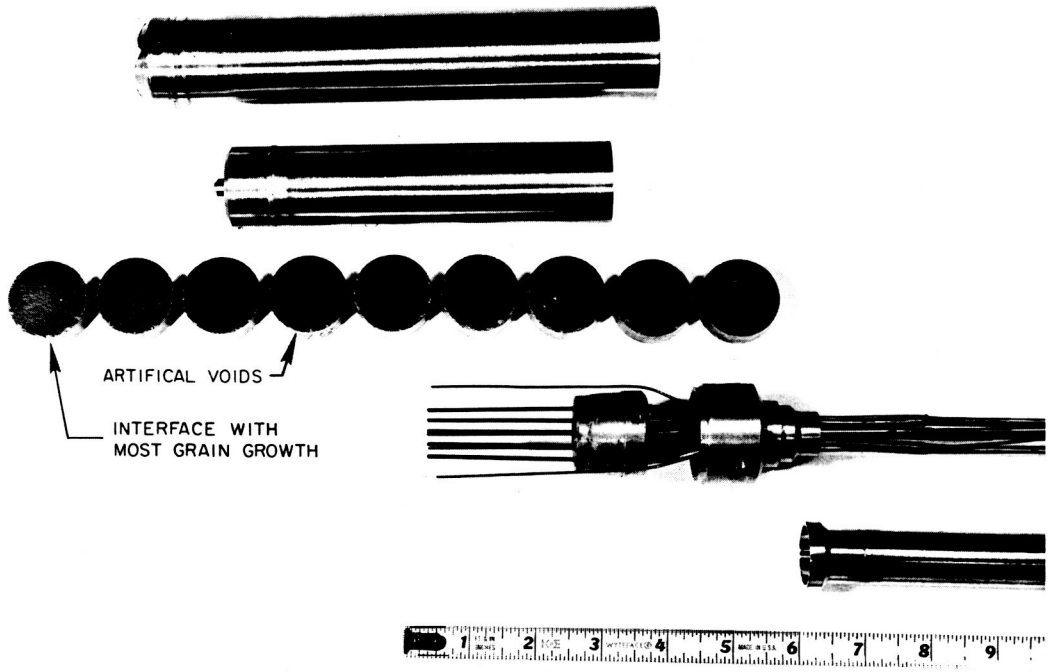

FIGURE 4 COMPONENTS INCLUDED IN THE IN-PILE THERMAL CONDUCTIVITY ASSEMBLY.

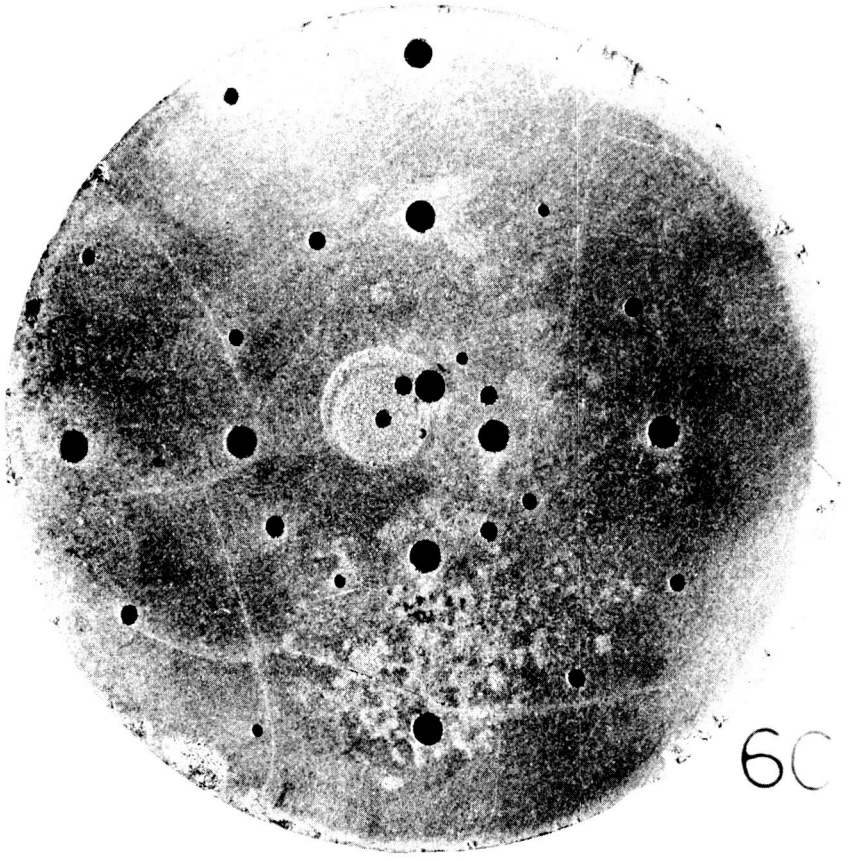

FIGURE 5A ARTIFICAL VOIDS ULTRASONICALLY DRILLED IN UO_2 PELLET BEFORE IRRADIATION. (PELLET DIAMETER = 1.25").

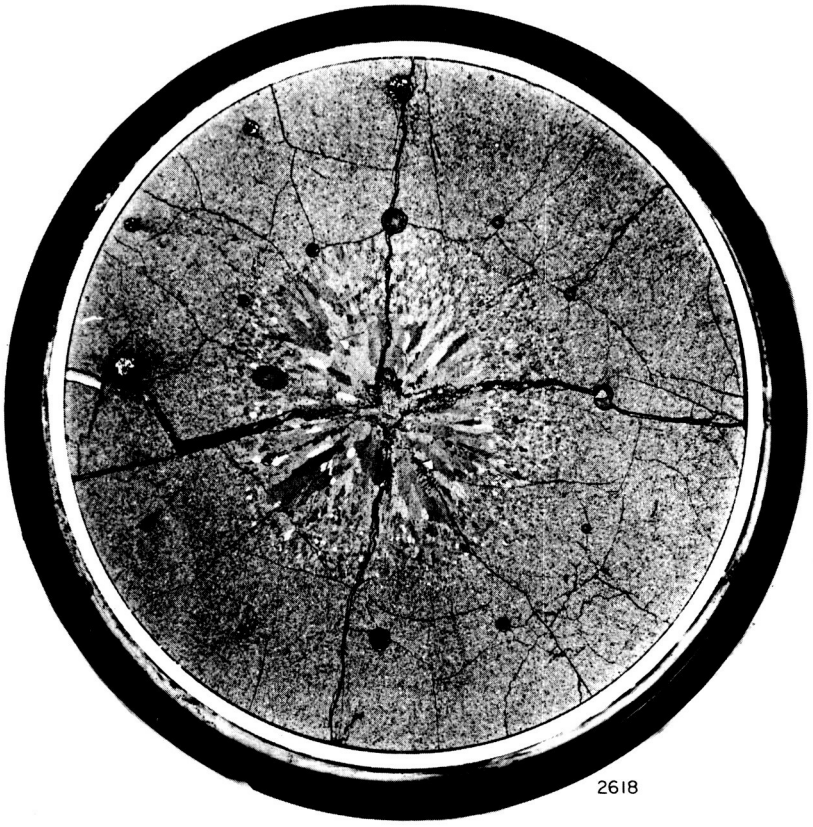

FIGURE 5B ARTIFICIAL VOIDS AFTER IRRADIATION.

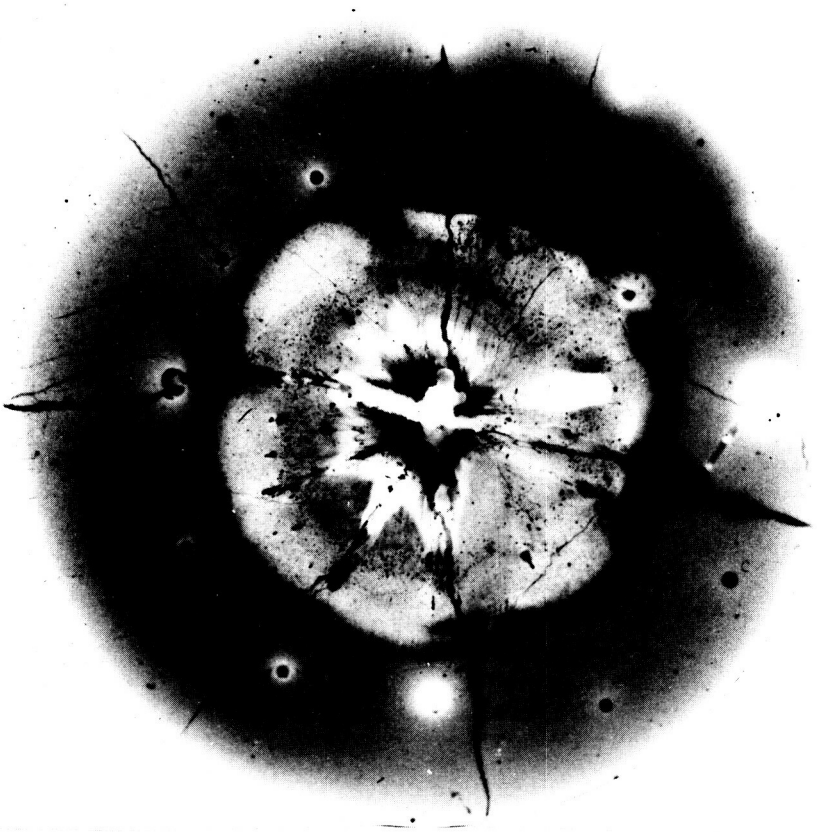

FIGURE 5C AUTORADIOGRAPH OF PELLET CONTAINING ARTIFICAL VOIDS.

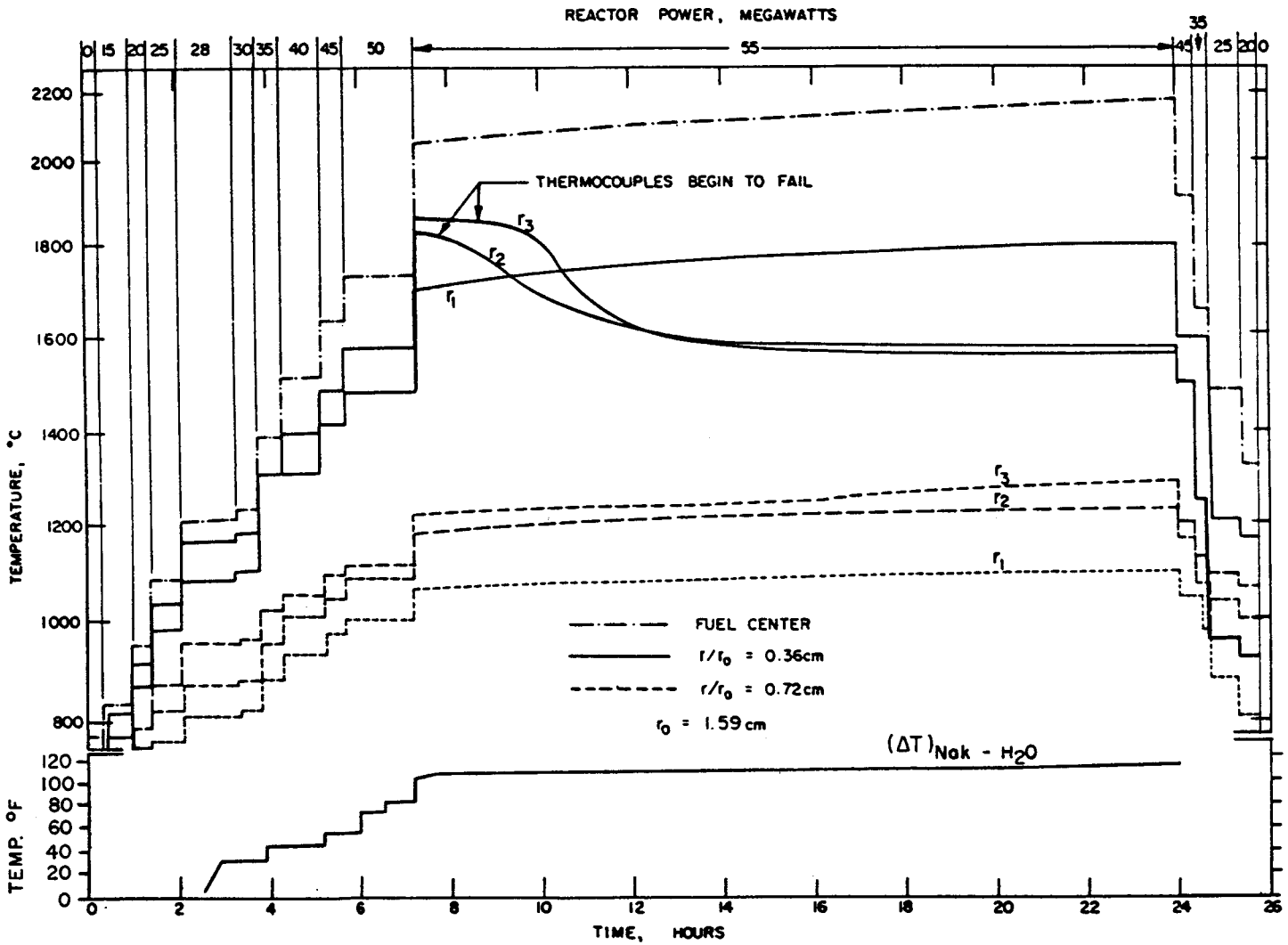

FIGURE 6 TEMPERATURE DISTRIBUTION IN UO_2 - THERMAL CONDUCTIVITY - CAPSULE I. (O/U = 2.005)

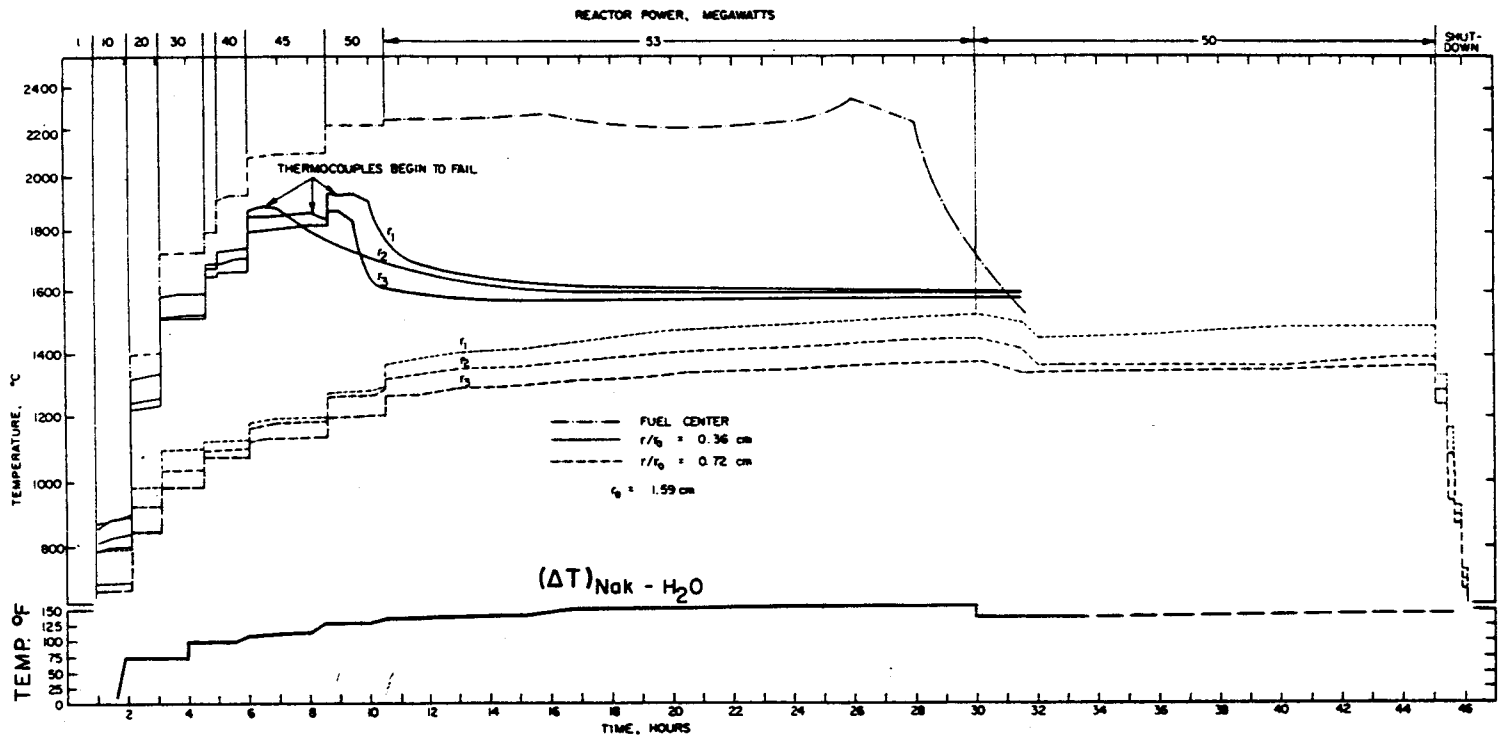

FIGURE 7 TEMPERATURE DISTRIBUTION IN UO_2 - THERMAL CONDUCTIVITY - CAPSULE II (O/U = 2.005)

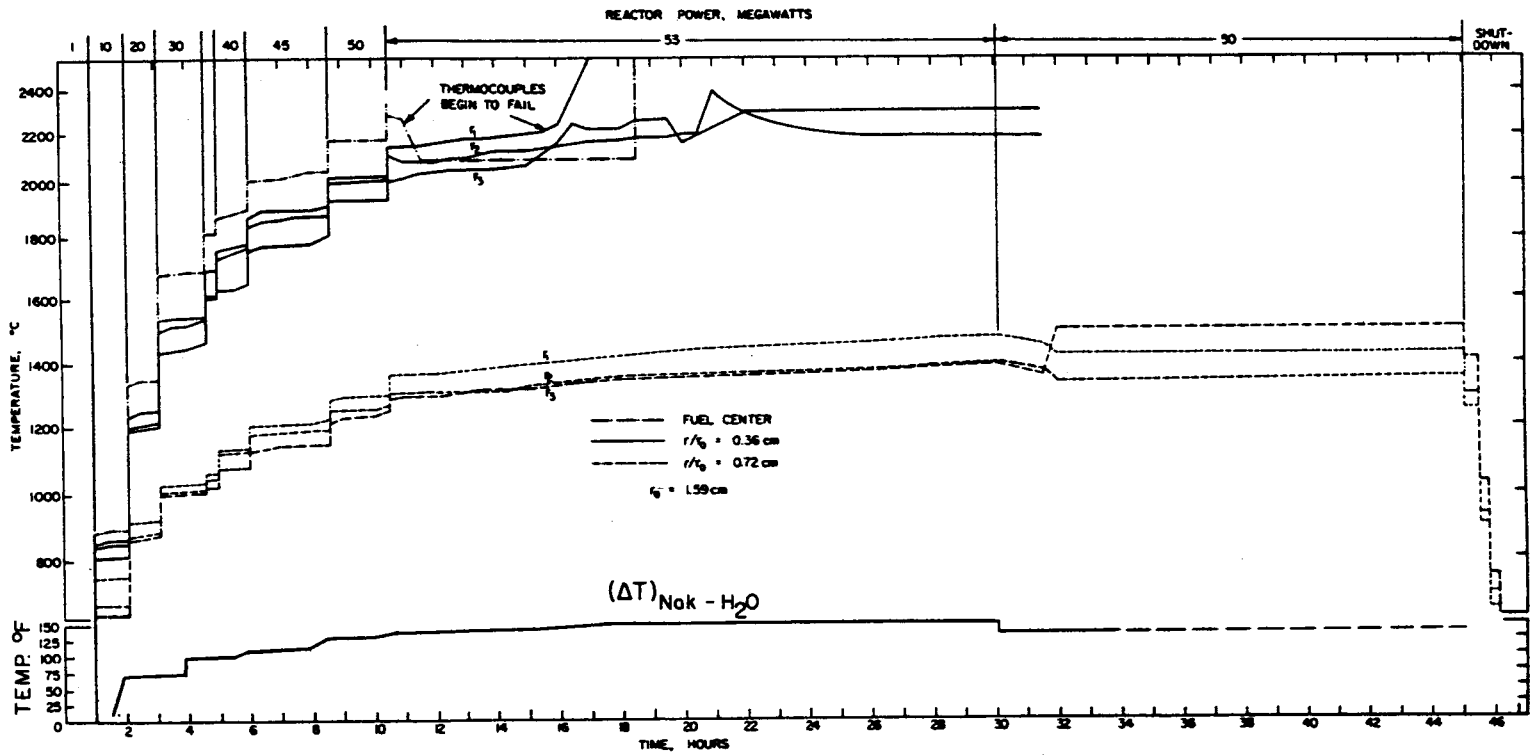

FIGURE 8 TEMPERATURE DISTRIBUTION IN UO_2 - THERMAL CONDUCTIVITY - CAPSULE III (O/U = 1.94)

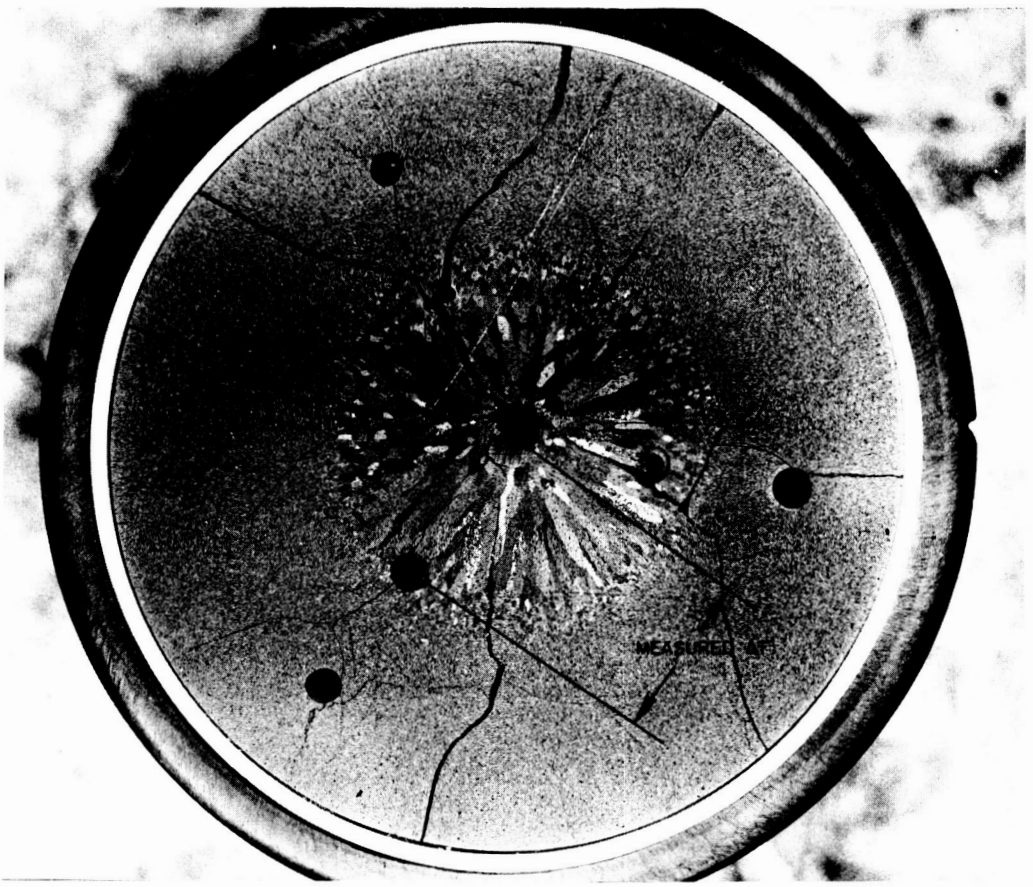

FIGURE 9 CAPSULE I FUEL SECTION AT THERMOCOUPLE HOT JUNCTION.

FUEL DIAMETER = 3.18 cm.

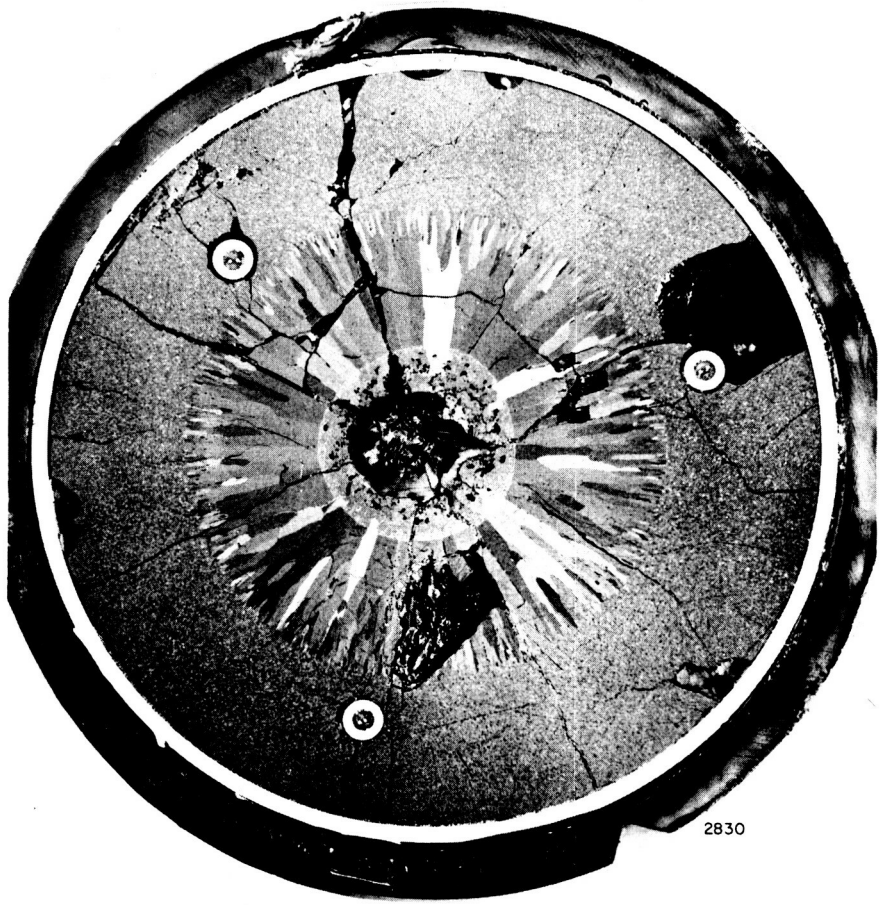

FIGURE 10 CAPSULE II CROSS SECTION AT THERMOCOUPLE HOT JUNCTIONS.

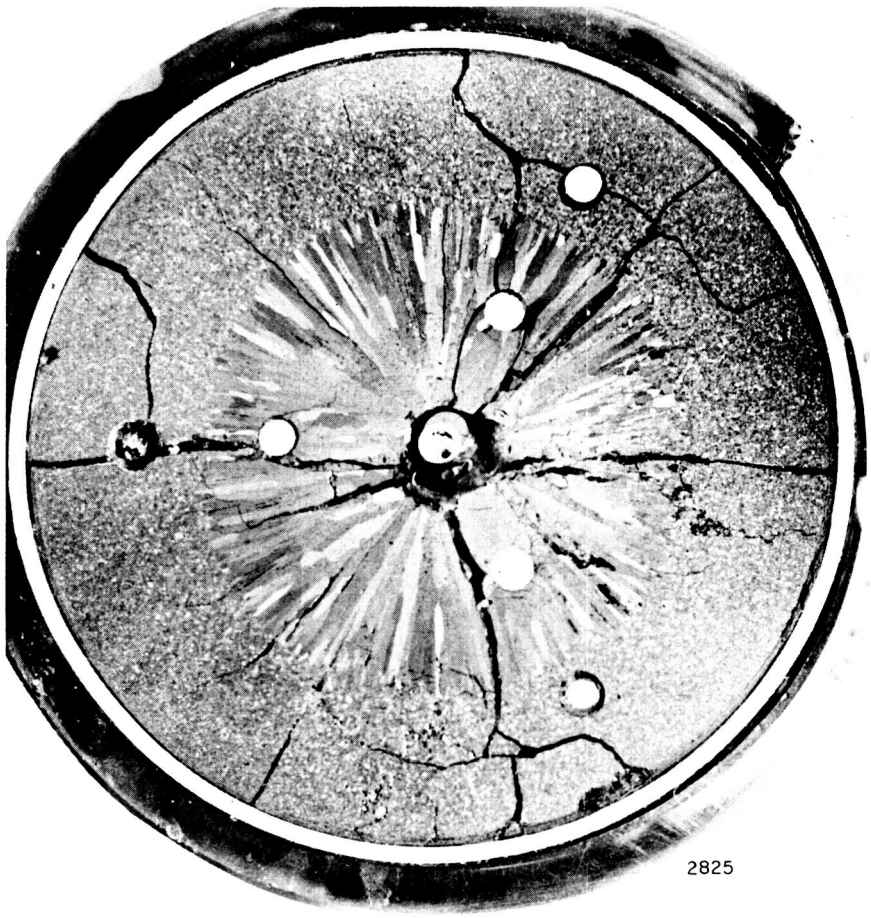

FIGURE 11 CAPSULE III CROSS SECTION AT THERMOCOUPLE HOT JUNCTIONS.

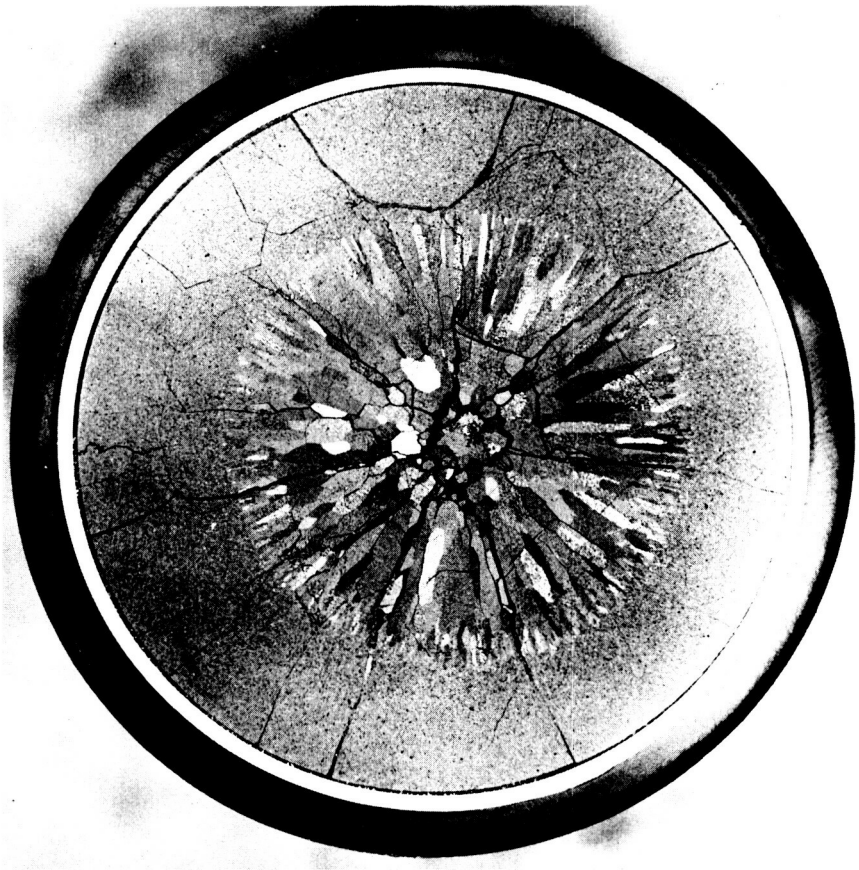

FIGURE 12 FUEL SECTION WITH MAXIMUM GRAIN GROWTH.

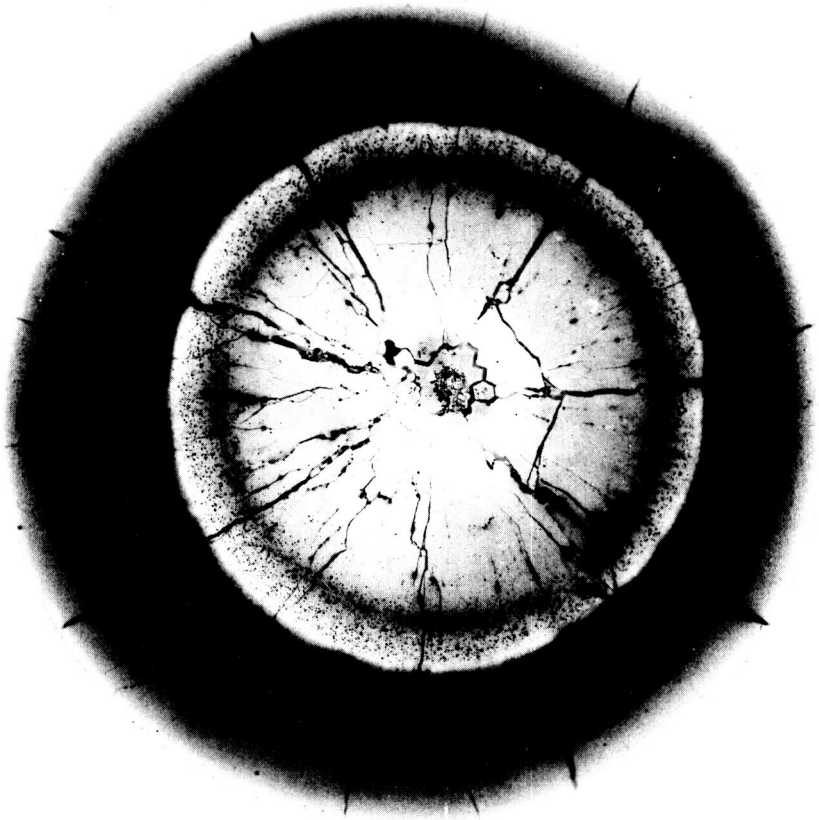

FIGURE 13 AUTORADIOGRAPH OF FUEL SECTION WITH MAXIMUM GRAIN GROWTH.

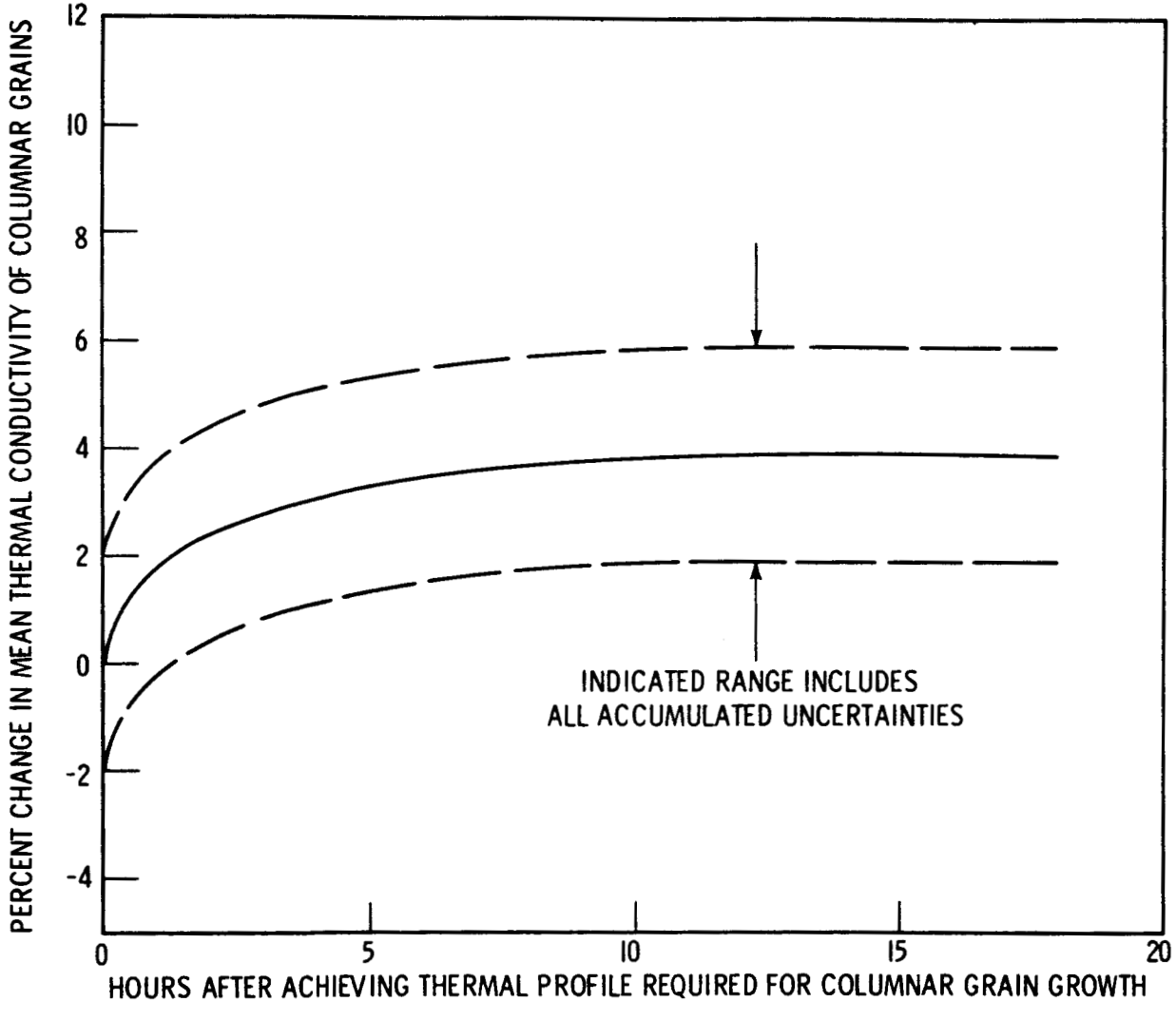

EFFECT OF COLUMNAR GRAIN GROWTH ON HEAT TRANSFER IN URANIUM DIOXIDE FUELS

FIGURE 14

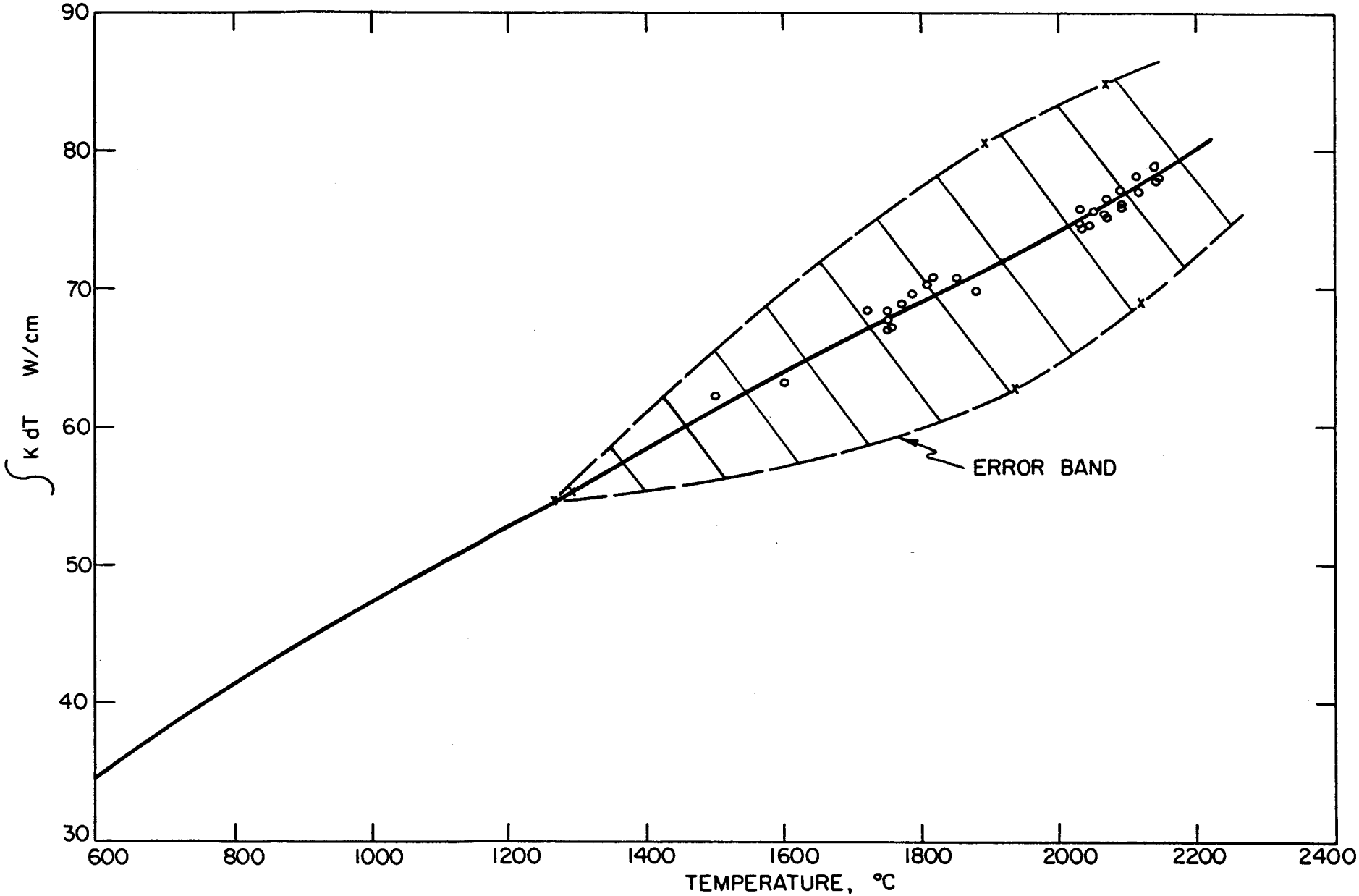

FIGURE 15 $\int KdT$ vs T: CAPSULE I ($UO_{2.005}$).

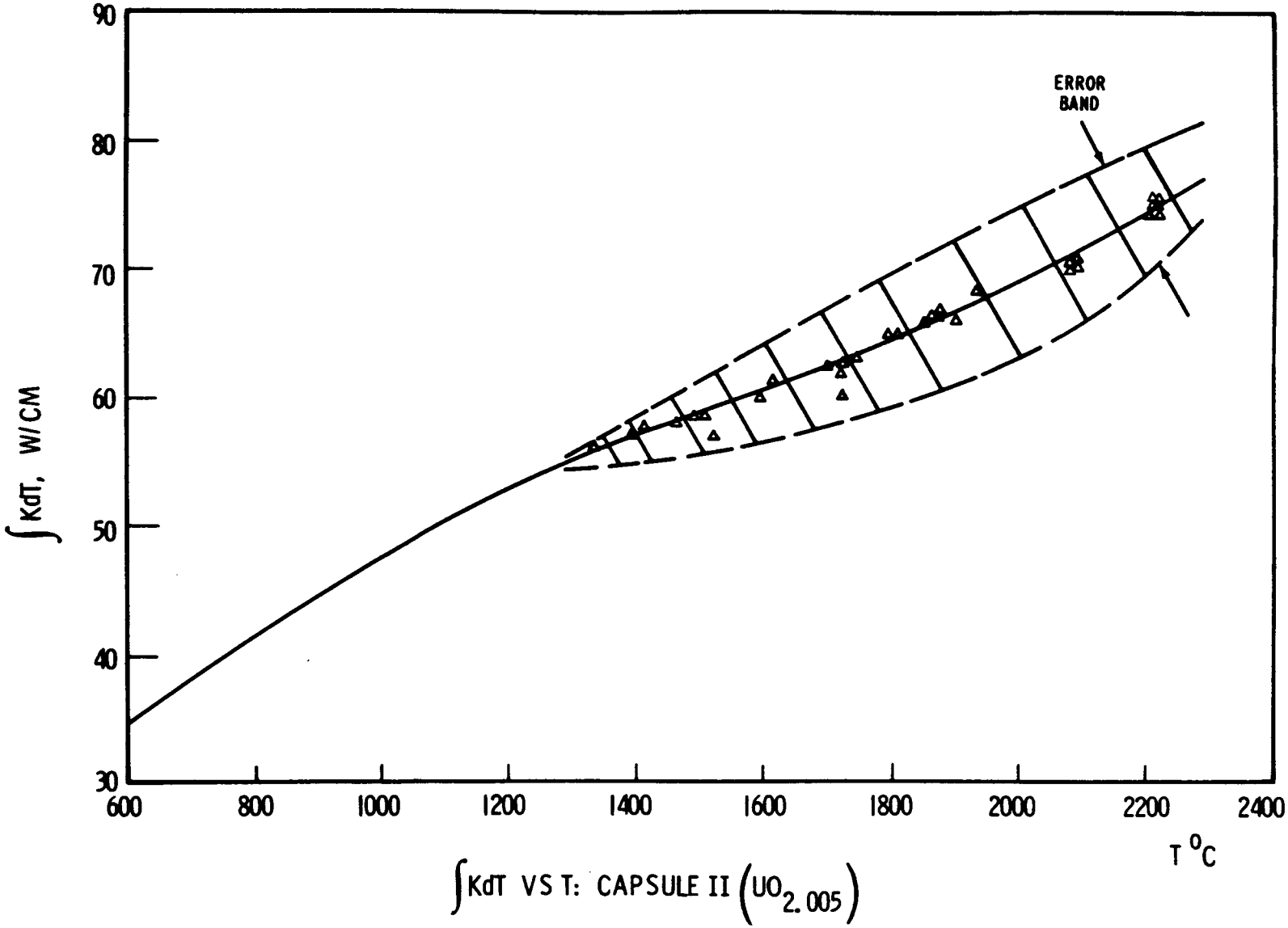

∫KdT VS T: CAPSULE II ($UO_{2.005}$)

FIGURE 16

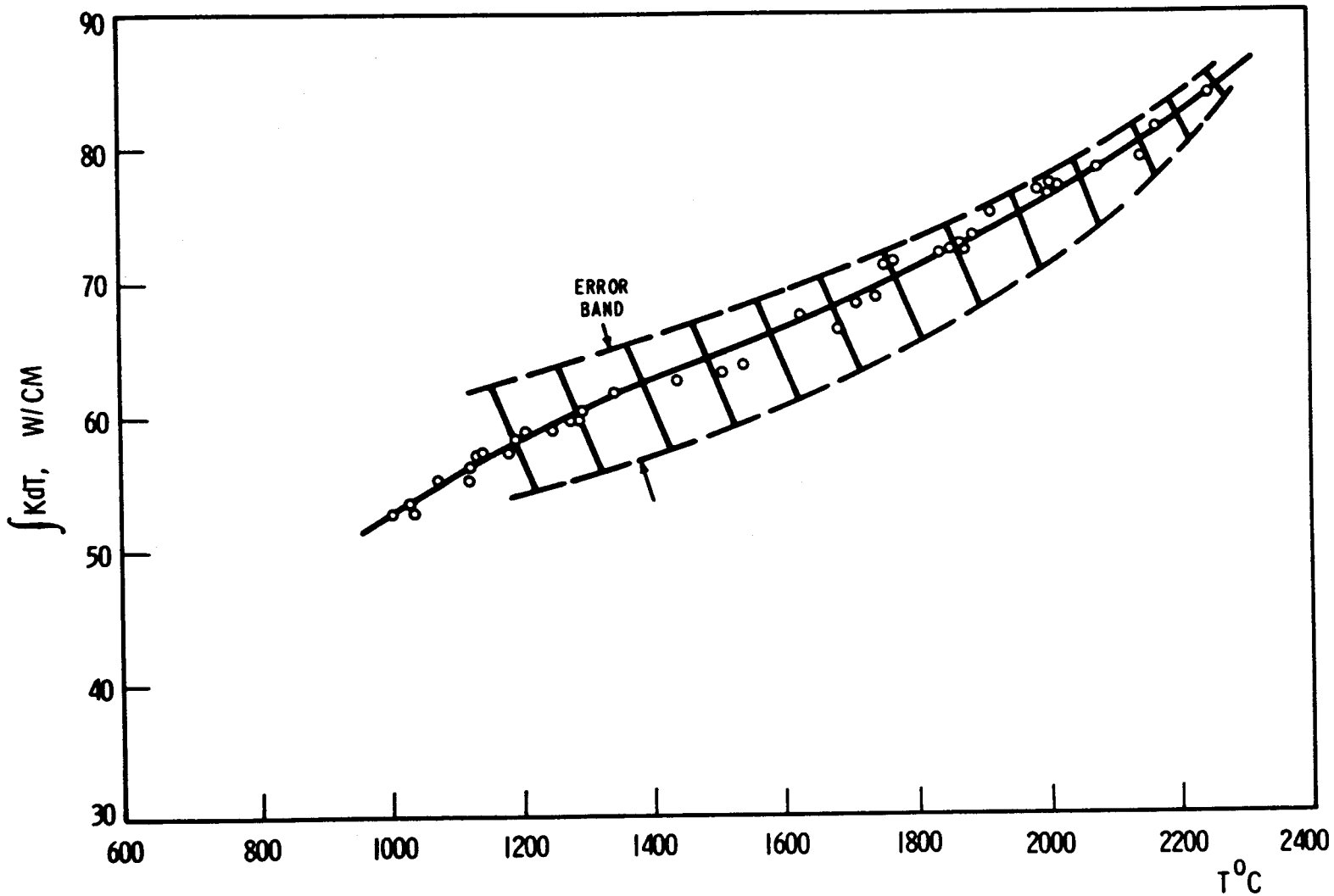

$\int KdT$ VS T: CAPSULE III $(UO_{1.941})$

FIGURE 17

NASA Distribution List

NASA-Lewis Research Center
21000 Brookpark Road
Cleveland, Ohio 44135

R. M. Caves	MS 105-1
D. C. DiIanni (3)	49-2
P. L. Donoughs	49-2
L. V. Humble	49-2
S. J. Kaufman	49-2
A. F. Lietzke	49-2
Dr. B. Lubarsky	500-201
J. F. Mondt	500-309
F. E. Rom	49-2
E. W. Sams	49-2
N. D. Sanders	302-1
N. R. Thielke	54-2
Report Control	5-5
Library (2)	3-7

NASA Lewis Research Center
Plum Brook Station
Sandusky, Ohio 44871

L. Homyak
R. J. Koch
Library (2)

AEC-NASA Space Nuc. Prop. Office
U. S. Atomic Energy Commission
Washington, D. C. 20545

F. C. Schwenk
J. J. Lynch

NASA Scientific & Technical Information Facility (6)
Box 5700
Bethesda, Maryland

U.S. AEC Technical Information Service (3)
P. O. Box 65
Oak Ridge, Tennessee

U. S. Atomic Energy Commission (3)
Technical Report Library
Washington, D. C. 20545